Inorganic Chemistry

Article

pubs.acs.org/IC

Activation of CH_4 by Th^+ as Studied by Guided Ion Beam Mass Spectrometry and Quantum Chemistry

Richard M Cox,[†] P. B. Armentrout,*[,†] and Wibe A. de Jong[‡]

[†]Department of Chemistry, University of Utah, Salt Lake City, Utah 84112-0850, United States

[‡]Lawrence Berkeley National Laboratory, One Cyclotron Road, Berkeley, California 94720, United States

Supporting Information

ABSTRACT: The reaction of atomic thorium cations with CH_4 (CD_4) and the collision-induced dissociation (CID) of $ThCH_4^+$ with Xe are studied using guided ion beam tandem mass spectrometry. In the methane reactions at low energies, $ThCH_2^+$ ($ThCD_2^+$) is the only product; however, the energy dependence of the cross-section is inconsistent with a barrierless exothermic reaction as previously assumed on the basis of ion cyclotron resonance mass spectrometry results. The dominant product at higher energies is ThH^+ (ThD^+), with $ThCH_3^+$ ($ThCD_3^+$) having a similar threshold energy. The latter product subsequently decomposes at still higher energies to $ThCH^+$ ($ThCD^+$). CID of $ThCH_4^+$ yields atomic Th^+ as the exclusive product. The cross-sections of all product ions are modeled to provide 0 K bond dissociation energies (in eV) of $D_0(Th^+–H) \geq 2.25 \pm 0.18$, $D_0(Th^+–CH) = 6.19 \pm 0.16$, $D_0(Th^+–CH_2) \geq 4.54 \pm 0.09$, $D_0(Th^+–CH_3) = 2.60 \pm 0.30$, and $D_0(Th^+–CH_4) = 0.47 \pm 0.05$. Quantum chemical calculations at several levels of theory are used to explore the potential energy surfaces for activation of methane by Th^+, and the effects of spin–orbit coupling are carefully considered. When spin–orbit coupling is explicitly considered, a barrier for C–H bond activation that is consistent with the threshold measured for $ThCH_2^+$ formation (0.17 ± 0.02 eV) is found at all levels of theory, whereas this barrier is observed only at the BHLYP and CCSD(T) levels otherwise. The observation that the CID of the $ThCH_4^+$ complex produces Th^+ as the only product with a threshold of 0.47 eV indicates that this species has a $Th^+(CH_4)$ structure, which is also consistent with a barrier for C–H bond activation. This barrier is thought to exist as a result of the mixed (^4F,^2D) electronic character of the Th^+ $J = {}^3/_2$ ground level combined with extensive spin–orbit effects.

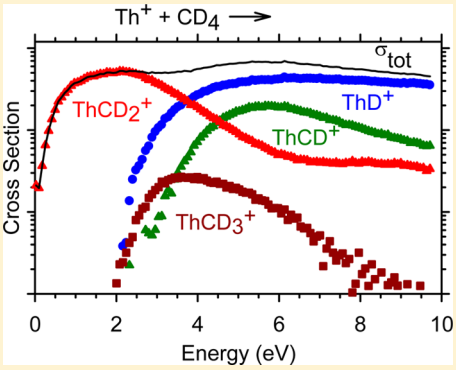

INTRODUCTION

The activation of methane by metals is an active area of research.[1−3] This interest is motivated in part by the desire to find more efficient or selective catalysts as well as to gain insight into the physical aspects involved in the C–H bond activation process at metal centers. Such insight would be useful because methane is relatively inert but is a plentiful feedstock in the synthesis of more complex hydrocarbons.[2,4] To this end, several groups, including our own, have looked at the reactions of methane with the atomic first-,[1,5−12] second-,[1,7,13−19] and third-row[1,7,20−30] transition metal cations. Others have investigated the same reaction for lanthanide[1,2,31−33] and actinide cations.[34−36]

The latter actinide studies were conducted using Fourier transform ion cyclotron resonance mass spectrometry (FT-ICR MS). This instrumentation has also been used to examine oxidation reactions of actinide cations, with thorium being established as the most reactive of the actinide series.[37,38] Actinide reactivity has been inversely correlated to the promotion energy from the ground level to the first level with two 6d electrons ($5f^{n-3}6d^27s$ or $5f^{n-2}6d^2$ configurations).[39,41] In these studies, the ground state of Th^+ was reported to have a $6d^27s$ (^4F) configuration, thus requiring no promotion.

Similar to the oxidation studies, thorium was also observed to be the most reactive of the actinides with several hydrocarbons studied using FT-ICR.[36] It is the only actinide to dehydrogenate methane at thermal energies, albeit with low efficiency, $k/k_{col} = 0.009 \pm 0.005$[36] and $k/k_{col} = 0.02 \pm 0.01$,[35] where the collision rate limit (k_{col}) is the rate derived from modified variational transition-state/classical trajectory theory.[40] Both studies interpreted their observations to indicate an exothermic reaction, which suggested that $D_0(Th^+–CH_2) \geq D_0(H_2C–H_2) = 457 \pm 1$ kJ/mol.

The reaction of thorium cation with methane has also been studied theoretically.[41,42] Two competing explanations for the low efficiency of the dehydrogenation pathway have emerged. In a reaction coordinate presented by di Santo et al.,[41] the reaction proceeds exclusively on the doublet spin surface, originating from a ^2F Th^+ ground state, with a small barrier of 4 kJ/mol at the transition state between the first two intermediates: $Th^+(CH_4)$, the association complex of the ion

Received: January 22, 2015
Published: March 13, 2015

DOI: 10.1021/acs.inorgchem.5b00137
Inorg. Chem. 2015, 54, 3584−3599

and methane formed through electrostatic interactions, and $HThCH_3^+$, the inserted species. These calculations used B3LYP in combination with a Stuttgart−Dresden effective core potential and basis set (SDD) for Th^+ and a 6-311++G(d,p) basis set for C and H. Such a barrier would indicate that only a small population of the reactants would have the necessary energy to react, consistent with the experimentally observed low efficiency. Another recent study[42] used the same Pople basis set for C and H and an unpublished double-ζ quality basis set in combination with the Stuttgart−Dresden ECP and the B3PW91 functional. Here, no barrier along the lowest energy pathway was observed, but a crossing was found between the quartet (the ground state of the Th^+ reactant in this study) and doublet (needed to form the ground state of $HThCH_3^+$) surfaces near the first intermediate. They concluded that the inefficiency at this crossing point hindered the crossover to the doublet surface on which the reaction evolves to products. In this study, the electronic state of the Th^+ reactant was not identified beyond its spin.

Despite these efforts, actinide chemistry (particularly in the gas phase) is largely unexplored. This is attributable, in part, to safety concerns, as all actinides except thorium and uranium are highly radioactive. This limits the ability to study most actinides to dedicated laboratories or theoretical studies. In order for theoretical methods to be accurate, reliable experimental benchmarks are critically needed. Here, we present a study of the activation of methane and its deuterated analogue by atomic thorium cations using guided ion beam tandem mass spectrometry (GIBMS). A key feature of GIBMS is the ability to control the kinetic energy of the reactant ion over 3 or more orders of magnitude in the laboratory frame. This allows for the determination of the energy dependence of the dehydrogenation reaction as well as the study of higher energy reaction pathways. To more fully explore this reaction surface experimentally, we also examine the collision-induced dissociation (CID) of the $ThCH_4^+$ cation. This experimental work is complemented by quantum chemical calculations performed here at several levels of theory and a careful quantitative evaluation of spin−orbit effects. A key objective of the present study is the determination of experimental bond dissociation energies (BDEs) from which theoretical methods can be evaluated more completely.

EXPERIMENTAL AND THEORETICAL METHODS

Instrument. The guided ion beam tandem mass spectrometer used in these studies has been described previously.[43] Briefly, Th^+ (^{232}Th 100% abundance) and $ThCH_4^+$ ions are created in a direct current discharge flow tube (DC/FT) source described further below.[44] Ions are extracted from the source, focused through a magnetic momentum analyzer where the reactant ion is mass-selected, and subsequently decelerated to a well-defined kinetic energy. These ions are passed into a radiofrequency (rf) octopole ion beam guide,[45−47] where the ions are radially trapped. The octopole passes through a static gas cell that contains the neutral reactant gas at pressures of 0.05−0.40 mTorr. Pressures are low to ensure that the probability of more than one collision occurring between the reactants is small. It is verified that the measured cross-sections reported below do not vary with neutral reactant pressure. After the collision cell, remaining reactant and product ions drift to the end of the octopole, are focused through a quadrupole mass filter for mass analysis, and are counted using a Daly detector.[48] Reaction cross-sections are calculated, as described previously, from product ion intensities relative to reactant ion intensities after correcting for ion intensities with the neutral gas no longer directed to the gas cell.[47] Uncertainties in the measured absolute cross-sections are estimated to be ±20%, with relative uncertainties of ±5%.

Laboratory ion energies (lab) are converted to the center-of-mass frame (CM) using the relationship $E_{CM} = E_{lab} \times m/(m + M)$, where m and M are the masses of the neutral and ionic reactants, respectively. The absolute zero of energy and the full width at half-maximum (fwhm) of the ion beam are determined by using the octopole guide as a retarding potential analyzer.[47] Typical fwhm's of the energy distribution for these experiments were 0.4−0.6 eV (lab). Uncertainties in the absolute energy scale are 0.1 eV (lab). All energies reported below are in the CM frame.

Ion Source. The DC/FT source is described in detail elsewhere.[44] Th^+ ions are created when Ar ionized by a dc electric field (2.5 kV) collides with a cathode holding the thorium powder sample. Ions typically thermalize under ∼10^5 collisions with the He/Ar carrier gases in a 9:1 mixture in a 1 m long flow tube. Total pressure in the flow tube is 0.2−0.5 Torr. $ThCH_4^+$ is created by leaking methane into the flow tube 15 cm downstream of the discharge through a variable leak valve. Previous experiments have indicated that atomic metal ions generated in the DC/FT source generally have internal electronic temperatures between 300 and 1100 K.[49−53] At 300 K, 99.99% of Th^+ is in its $J = {}^3/_2$ ground level.[54,55] At 1100 K, 76% of Th^+ is in the ground level with an average electronic energy of only 0.05 eV (see Table S1). For the $ThCH_4^+$ complex, the ions are expected to have an internal temperature of 300 K.

Data Analysis. The kinetic energy dependence of endothermic reactions is modeled using eq 1[46,56,57]

$$\sigma(E) = \sigma_0 \sum g_i (E + E_i - E_0)^n / E \quad (1)$$

where σ_0 is an energy-independent scaling factor; E is the relative kinetic energy of the reactants; E_i is the internal energy of the reactants' electronic, vibrational, and rotational states having populations g_i($\sum g_i = 1$); n is an adjustable parameter; and E_0 is the 0 K reaction threshold. Before comparison to the data, eq 1 is convoluted over the kinetic energy distributions of the reactants.[47,58,59] The σ_0, n, and E_0 parameters are then optimized using a nonlinear least-squares method to best reproduce the experimental cross-section. Uncertainties in E_0 are calculated from the threshold values for several independent data sets over a range of n values combined with the absolute uncertainties in the kinetic energy scale and internal energies of reactant ions. Calculated thresholds are then used to determine bond dissociation energies (BDEs), $D_0(Th^+–L)$, using relationship 2.

$$D_0(Th^+–L) = D_0(L–R) - E_0 \quad (2)$$

This equation assumes that there are no barriers in excess of the endothermicity of the reaction. When evidence of a barrier exists, then eq 2 provides a lower limit to the true BDE. Neutral BDEs, $D_0(L–R)$, were taken from thermochemistry found in the NIST webBook[60] or previous compilation.[22] Thermodynamic values used to determine neutral BDEs are listed in Table S2 of the Supporting Information.

Theoretical Calculations. Most of the quantum chemical calculations were performed using the Gaussian 09 suite of programs.[61] Geometries of all intermediates and transition states were optimized using the B3LYP[62,63] functional with a Stuttgart−Dresden small core (60 electron) relativistic effective core potential (ECP) and accompanying basis set (SDD)[64] for Th^+ and the Pople basis set[65] 6-311++G(d,p) for C and H. This SDD basis set is the 1997 revision made by the Stuttgart/Dresden groups and can be obtained from the EMSL basis set exchange.[66,67] Single-point energies were then calculated using several density functional theory (DFT) approaches: B3LYP, B3PW91, and BHandHLYP (BHLYP) functionals with the SDD basis set for Th^+ and a 6-311++G(3df,3p) basis set for C and H that has been shown to be reasonably accurate in studies of third-row transition metal−methane systems by our group.[25,28,29,68−70] Additional single-point calculations using the B3LYP/SDD/6-311++G(d,p) structures were performed using a (14s13p10d8f6g)/[6s6p5d4f3g] atomic natural orbital basis set of quadruple-ζ quality with the SDD small core ECP (ANO) and a (14s13p10d8f6g)/[10s9p5d4f3g] segmented basis set of quadruple-ζ

DOI: 10.1021/acs.inorgchem.5b00137
Inorg. Chem. 2015, 54, 3584−3599

quality with the SDD small core ECP (Seg. SDD) for Th along with a 6-311++G(3df,3p) basis set for C and H.[71] Unless noted otherwise, all theoretical energies reported below are calculated using Seg. SDD/6-311++G(3df,3p) basis sets for Th^+/C and H. Other groups have indicated that the B3PW91 has performed well in the study of other actinide systems.[42] Holthausen et al.[72] previously considered the appropriate choice of level of theory to study first- and third-row transition metal methyl cation species and concluded that BHLYP performed well for singly bound species. This conclusion has been confirmed in subsequent use by our group, namely, that BHLYP performs well for several third-row transition metal hydride systems; however, BHLYP is not accurate for species having more than a single covalent bond.[69,70] Additionally, single-point energies were calculated using the coupled cluster method that mixes in single and double excitations and perturbative triple excitations with the Th^+ (5s,5p) and the C (1s) orbitals frozen for electron correlation, CCSD(T).[65,73−75] For all open-shell calculations, unrestricted open-shell wave functions were utilized throughout. With a few exceptions that are explicitly noted, spin contamination is insignificant. All single-point energies were zero-point energy-corrected using the frequencies of the optimized structures after scaling by 0.989.[76] Transition states were found by employing a synchronous transit-guided quasi-Newton (STQN) method[77,78] to approach the quadratic region around the transition state. Transition states were checked to ensure that there was only one imaginary frequency, which led to the appropriate intermediates or products. BDEs of the reaction products were also calculated from these various single-point energies.

Additional calculations were performed using the NWChem computational chemistry software.[79] Here, the geometries were optimized using the PBE0 functional using the latest Stuttgart−Cologne ECP[80] with a newly developed correlation consistent type basis set for Th (20s17p12d11f5g3h1i)/[7s7p6d5f5g3h1i] developed by K.A. Peterson (KAP).[81] For C and H, the cc-pVTZ basis sets[82] were used. All geometries used in NWChem were optimized using the PBE functional.[83] The nudged elastic band method[84] was used to locate transition states, and saddle point optimizations and frequency calculations were used to ensure a transition state with one imaginary frequency was found. It should be noted that although different basis sets and functionals were used in the Gaussian and NWChem calculations the resulting structures were found to be very similar (as detailed in Table S6 of the Supporting Information). Single-point energies were calculated using the CCSD(T) method. As with the Gaussian calculations, the Th^+ (5s,5p) and the C (1s) orbitals were frozen. For CCSD(T), a spin-restricted open-shell wave function was used as a reference for the correlated calculations based on an unrestricted formulation.

EXPERIMENTAL RESULTS

$Th^+ + CH_4$ (CD_4). The reaction of Th^+ with methane yields products formed in reactions 3−6.

$$Th^+ + CH_4 \rightarrow ThCH_2^+ + H_2 \quad (3)$$

$$\rightarrow ThH^+ + CH_3 \quad (4)$$

$$\rightarrow ThCH_3^+ + H \quad (5)$$

$$\rightarrow ThCH^+ + H + H_2 \quad (6)$$

The cross-sections for these reactions are shown in Figure S1 in the Supporting Information and are very similar to the analogous methane-d_4 reaction cross-sections shown in Figure 1. Mass overlap for the $ThCH_3^+$ and $ThCH^+$ products with the more intense $ThCH_2^+$ product was observed. In both cases, cross-sections were corrected to remove overlap from adjacent mass peaks, a procedure that was straightforward and unambiguous because of the different energy dependences of the products in question. The reactions with methane-d_4

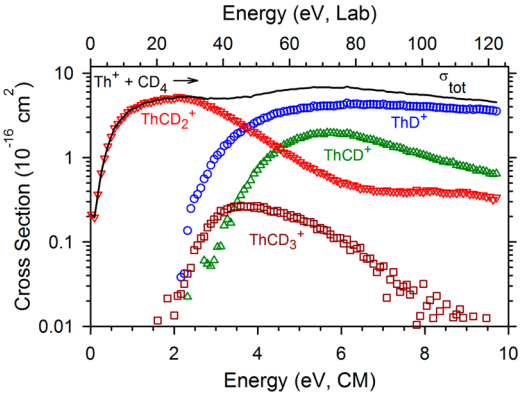

Figure 1. Cross-sections for the reaction between Th^+ and CD_4 as a function of energy in the CM (lower x axis) and lab (upper x axis) frames.

showed much less mass overlap. In all cases, the cross-sections produced in reactions 3−6 for both methane and methane-d_4 are similar in energy dependence and magnitude.

At low energy, reaction 3 dominates with a cross-section that initially rises with increasing energy. The energy dependence of reaction 3 is inconsistent with that of a barrierless exothermic reaction, as was concluded from the FT-ICR studies.[35,36] A plot of our experimental data for reaction 3 converted to a rate coefficient as a function of kinetic energy according to a method outlined elsewhere[47] is presented in Figure 2. For CH_4,

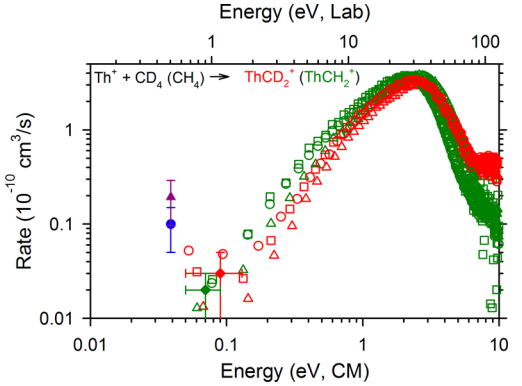

Figure 2. Reaction rate for $Th^+ + CD_4$ (CH_4) → $ThCD_2^+$ ($ThCH_2^+$) + D_2 (H_2) plotted as a function of kinetic energy. Present work is in red ($ThCD_2^+$) and green ($ThCH_4^+$). Average rates at 700 ± 300 K for $ThCD_2^+$ (red diamond) and 500 ± 150 K for $ThCH_2^+$ (green diamond). FT-ICR results from Gibson et al.[36] (blue circle) and Marçalo et al.[35] (purple triangle). Lab frame shown corresponds to the CD_4 reaction.

it can be seen that at the lowest energies in the present experiment (0.07 ± 0.02 eV, equivalent to a temperature of 500 ± 150 K) we do observe a small amount of product with a rate constant of 0.02 ± 0.01 × 10^{-10} cm^3/s and a reaction efficiency of k/k_{col} = 0.002 ± 0.001, where the collision limit is defined by the Su−Chesnavich variational transition-state/classical trajectory theory rate constant.[40] Likewise, the rate coefficient for reaction 3 with CD_4 is 0.03 ± 0.02 × 10^{-10} cm^3/s at our lowest energies (0.09 ± 0.04 eV, equivalent to an average temperature of 700 ± 300 K). At this same temperature, the rate coefficient for reaction 3 with CH_4 is 0.04 ± 0.03 × 10^{-10} cm^3/s. The slight differences between the rates observed in reaction 3 using CH_4 and CD_4 can be explained by two effects. The first takes

DOI: 10.1021/acs.inorgchem.5b00137
Inorg. Chem. 2015, 54, 3584−3599

Table 1. Fitting Parameters of Equation 1 for the Indicated Reaction Cross-Section

reaction[a]	σ_0	n	E_0 (eV)
$Th^+ + CH_4 \rightarrow ThH^+ + CH_3$	11 ± 3	1.2 ± 0.1	2.38 ± 0.16
	(7.0 ± 0.8)	(1.4 ± 0.2)	(2.25 ± 0.08)
$Th^+ + CH_4 \rightarrow ThCH^+ + H_2 + H$	2.1 ± 0.1	0.8 ± 0.2	3.08 ± 0.17
	(2.3 ± 0.2)	(1.8 ± 0.1)	(2.98 ± 0.06)
$Th^+ + CH_4 \rightarrow ThCH_2^+ + H_2$	6.6 ± 0.3	1.5 ± 0.1	0.17 ± 0.02
	(6.6 ± 0.1)	(1.4 ± 0.1)	(0.28 ± 0.03)
$Th^+ + CH_4 \rightarrow ThCH_3^+ + H$	0.9 ± 0.3	1.6 ± 0.4	2.11 ± 0.15
	(1.2 ± 0.4)	(2.0 ± 0.4)	(2.13 ± 0.11)
$ThCH_4^+ + Xe \rightarrow Th^+ + CH_4$[b]	3.0 ± 0.3	1.8 ± 0.2	0.46 ± 0.05
	[3.1 ± 0.4]	[1.7 ± 0.2]	[0.47 ± 0.05]

[a]Values in parentheses are for the analogous reaction with CD_4. Uncertainties are 1 standard deviation of the mean. [b]Values in brackets include lifetime effects by incorporating RRKM theory.[91,92]

into account that the collisional rate coefficient depends inversely on the square root of the reduced mass of the reactants, 15.00 u for CH_4 and 18.46 u for CD_4, such that the CD_4 collision rate is 90% of that for CH_4. The second relates to the differences in zero-point energy (ZPE) between the two reactants. As a result, $D_0(D_2C{-}D_2)$ is slightly stronger than $D_0(H_2C{-}H_2)$ so that the threshold for reaction 3 with CD_4 is higher than with CH_4.

Previously, Marçalo et al.[35] and Gibson et al.[36] observed that Th^+ reacts with CH_4 with rates of $0.20 \pm 0.10 \times 10^{-10}$ cm^3/s for an efficiency of $k/k_{col} = 0.02 \pm 0.01$ and $0.10 \pm 0.05 \times 10^{-10}$ cm^3/s for an efficiency of $k/k_{col} = 0.009 \pm 0.005$, respectively, in ICR experiments at nominally room temperature. Both ICR rates are larger than that measured here, but they are of similar magnitude and nearly within the combined uncertainties, Figure 2. It seems plausible that the ICR rates are somewhat elevated because the reactants have an effective temperature (electronic or translational) above 300 K.

The $ThCH_2^+$ ($ThCD_2^+$) cross-section rises until ~2 eV, where it begins to fall off, Figures S1 (1). This decline corresponds with the apparent thresholds for ThH^+ (ThD^+) and $ThCH_3^+$ ($ThCD_3^+$). Because decomposition of $ThCH_2^+$ ($ThCD_2^+$) to ThH^+ (ThD^+) cannot occur until much higher energies, this decline can be explained only by a shared common intermediate between the three channels. In addition, the peak in the magnitude of the $ThCH_3^+$ ($ThCD_3^+$) cross-section corresponds to the rise of the $ThCH^+$ ($ThCD^+$) cross-section, indicating that this latter product is formed by the dehydrogenation of $ThCH_3^+$ ($ThCD_3^+$). Finally, the $ThCH_3^+$ ($ThCD_3^+$) product can decompose by H (D) atom loss, which can be seen as the faster decline in the $ThCH_3^+$ ($ThCD_3^+$) cross-section starting near 6 eV and the plateau in the $ThCH_2^+$ ($ThCD_2^+$) cross-section starting at the same energy. The potential product, ThC^+, was also explicitly looked for but not observed.

The parameters used in eq 1 to model the experimental cross-sections are found in Table 1. Each channel was modeled independently. Because eq 1 explicitly includes the rotational, vibrational, and translational energy distributions of the reactants, the E_0 threshold energies determined correspond to 0 K values. Therefore, all BDEs determined below using eq 2 are 0 K dissociation energies.

$ThCH_4^+$ + Xe. The CID reaction of the $ThCH_4^+$ complex yields a single product, the atomic thorium cation, reaction 7, as shown in Figure 3.

$$ThCH_4^+ + Xe \rightarrow Th^+ + CH_4 + Xe \quad (7)$$

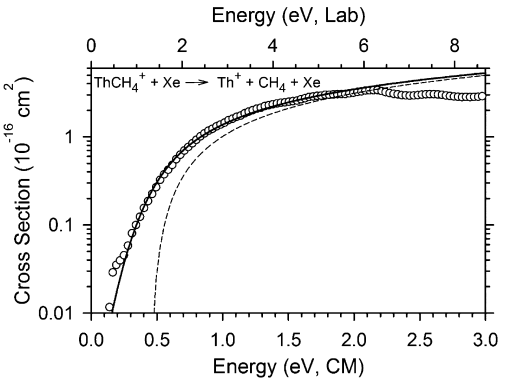

Figure 3. Cross-section for the collision-induced dissociation reaction of $ThCH_4^+$ with Xe. The best model of the data using parameters of eq 1 found in Table 1 is shown as a dashed line. The solid line shows this model convoluted over the kinetic and internal energy distributions of reactants at 300 K.

Other products explicitly looked for but not observed were ThH^+, $ThCH_3^+$, and $ThCH_2^+$, species that would indicate a structure of $HThCH_3^+$ or $H_2ThCH_2^+$. As discussed in more detail below, the $HThCH_3^+$ structure is the global minimum along the methane activation reaction pathway. In previous work,[22] the CID of $PtCH_4^+$ yielded both Pt^+ and PtH^+ products, indicating that the reactant had a $HPtCH_3^+$ structure (again the global minimum structure). Because the CID products expected from this inserted structure are not observed in the thorium system, the present CID results suggest that this species has a $Th^+(CH_4)$ structure. This is also confirmed by the comparison of the threshold energy obtained from analysis of this cross-section, Table 1, with theoretical values for the two possible structures. The evidence for this structural identification is discussed further below.

THERMOCHEMICAL AND THEORETICAL RESULTS

Th^+ Ground State. Some ambiguity surrounds the ground state of Th^+ because there is considerable interaction between the $^2D(6d7s^2)$ and $^4F(6d^27s)$ states. The $J = {}^3/_2$ ground level is identified as having mixed character, 43% $^4F(6d^27s)$ and 27% $^2D(6d7s^2)$.[54] A detailed list of the levels, including energies and character, chosen as representative of each state listed in Table 2 can be found in Table S1 in the Supporting Information. For the purpose of comparing the theoretical energies of each state, which are averaged over all spin–orbit levels, to the experimental results, the ground level is assigned as $^4F_{3/2}$. Despite the assignment of the ground level as part of the ^4F

DOI: 10.1021/acs.inorgchem.5b00137
Inorg. Chem. 2015, 54, 3584–3599

Table 2. Comparison of Theoretically Computed Excited State Energies (eV) to Spin−Orbit Averaged Experimental Values

state	experimental[a]	CCSD(T)[b]	B3LYP[b]	B3PW91[b]	BHLYP[b]
^{2}D ($6d7s^2$)	0.00	**0.00 (0.00)**	0.20	0.004	**0.00**
^{4}F ($6d^27s$)	0.06	0.19 (0.12)	0.38	0.02	0.18
^{2}F ($5f^27s$)	0.43	0.58	**0.00**	**0.00**	0.19
^{4}H (5f6d7s)	0.67	1.26	0.46	0.15	0.60
^{4}F ($6d^3$)	0.81	1.08	1.12	0.66	0.88

[a]Spin−orbit averaged values.[54,55] The choice of levels used for each state is explained in the Supporting Information. [b]Calculated using (14s13p10d8f6g)/[10s9p5d4f3g] segmented basis set with SDD ECP. Values in parentheses calculated using (20s17p12d11f5g3h1i)/[7s7p6d5f5g3h1i] basis with Stuttgart−Cologne ECP (KAP).

Table 3. Comparison of Experimental and Theoretical Bond Dissociation Energies (eV) without and (with) Spin−Orbit Corrections

		experimental		theoretical[a]				
bond	state	this work	literature	CCSD(T)[b]	CCSD(T)[c]	B3LYP	B3PW91	BHLYP
Th^+−H[d]	$^3\Delta_1$[e]	≥2.25 ± 0.18	2.46 ± 0.07[f]	2.91 (**2.69**)	2.79 (**2.57**)	**3.16 (2.94)**	**3.18 (2.96)**	**2.99 (2.77)**
	$^1\Sigma^+$			**2.95** (2.55)	**2.87** (2.47)	2.86 (2.46)	2.66 (2.26)	2.71 (2.31)
Th^+−CH[d]	$^1\Sigma^+$	6.19 ± 0.16		6.38 (5.98)	6.04 (5.64)	6.20 (5.80)	6.61 (6.21)	5.57 (5.17)
Th^+−CH_2[d]	^{2}A′	≥4.54 ± 0.09	≥4.74 ± 0.02[g]	5.34 (4.94)	5.14 (4.74)	5.32 (4.92)	5.44 (5.04)	4.82 (4.42)
Th^+−CH_3[d]	^{3}E[e]	≥2.39 ± 0.22		3.44 (**3.22**)	3.17 (2.95)	**3.35 (3.13)**	**3.54 (3.32)**	**2.98 (2.76)**
		2.60 ± 0.30[h]						
	$^1A_1$			**3.62 (3.22)**	**3.40 (3.00)**	3.29 (2.89)	3.25 (2.85)	2.96 (2.56)
Th^+−CH_4[i]	^{2}A/(^{4}A″)	0.47 ± 0.05		0.41 (0.51)	0.36 (0.49)	0.56 (0.51)	0.64 (0.57)	0.33 (0.43)
MAD[j]				0.44 (0.28)	0.37 (0.27)	0.39 (0.36)	0.56 (0.34)	0.42 (0.38)

[a]Values are relative to Th^+ (^{2}D, $6d7s^2$). Values in parentheses are relative to Th^+ ($^4F_{3/2}$, $6d^27s$) and include estimated spin−orbit corrections. Structures optimized (except CCSD(T)) at the indicated level of theory using Seg. SDD for Th^+ and a 6-311++G(3df,3p) for C and H; see the text. For ThH^+ and $ThCH_3^+$, the calculated ground state is in bold. [b]CCSD(T)/KAP/cc-pVTZ single-point calculations using PBE0/KAP/cc-pVTZ optimized structures. [c]CCSD(T)/Seg. SDD/6-311++G(3d,3p) single-point calculations using B3LYP/Seg. SDD/6-311++G(3df,3p) optimized structures. [d]Spin−orbit correction of −0.40 eV, the empirical difference between the ^{2}D state averaged over all spin−orbit levels and the ground $^4F_{3/2}$ level. [e]Spin−orbit correction of 0.18 eV for stabilization of $^3\Delta_1$ state. See the text. [f]Ref 87. [g]Result based on FT-ICR results.[35,36] Utilizes updated $D_0(H_2C{-}H_2)$ = 4.74 ± 0.02 eV.[60] [h]Includes correction for competition. See the text. [i]Value in parentheses corresponds to the ^{4}A″ ground state after including spin−orbit effects. See the text and Figure 4. [j]Mean absolute deviation of ground state theoretical BDEs from the experimental values excluding $ThCH_2^+$. Values in parentheses correspond to MADs after inclusion of spin−orbit estimates.

state, after averaging over all spin−orbit levels, the experimental ground state is ^{2}D. Experimental energies, averaged over properly weighted spin−orbit levels, for each low-lying state are listed in Table 2, as are theoretical energies of these states. Both BHLYP and CCSD(T) correctly identify the ground state as a ^{2}D ($6d7s^2$), whereas B3LYP and B3PW91 prefer the ^{2}F ($5f^27s$) state. At all levels of theory, considerable spin contamination, $s(s + 1) \sim 1.5$, is observed for the ^{2}D state, consistent with mixing in ^{4}F character. Overall, the BHLYP and CCSD(T) calculations do a particularly good job of reproducing the experimental values. When using the SDD and ANO basis sets, results are similar to those observed using the Seg. SDD basis set and can be found in Table S3. The use of the larger basis sets does significantly improve the results of the CCSD(T) calculations compared to experiment. Notably, the largest basis set, KAP, correctly predicts the order of the ^{2}D and ^{4}F states and yields the best agreement with experiment, Table 2.

Given that the ^{2}D ($6d7s^2$) state is the calculated ground state for Th^+ using CCSD(T) and BHLYP, all theoretical BDEs are determined here relative to this ^{2}D state in the next several sections. Consideration of spin−orbit interactions are needed to properly reference these BDEs to the $^4F_{3/2}$ ground level and are discussed later.

$ThCH_2^+$. The threshold measured for reaction 3 is 0.17 ± 0.02 eV, Table 1. Combined with $D_0(H_2C{-}H_2)$ = 4.74 ± 0.02 eV,[60] this would yield a BDE of $D_0(Th^+{-}CH_2)$ = 4.57 ± 0.06 eV if the threshold corresponds to the product asymptote. Similarly, the threshold for the deuterated system is 0.28 ± 0.03 eV, which would lead to $D_0(Th^+{-}CD_2)$ = 4.54 ± 0.06 eV. After accounting for the zero-point energy differences of 0.03 eV, the weighted average is $D_0(Th^+{-}CH_2)$ = 4.54 ± 0.09 eV, where the uncertainty is 2 standard deviations of the mean. This result is significantly different than the lower limit, $D_0(Th^+{-}CH_2) \geq$ 4.74 eV,[60] reported by Marçalo et al.[35] and Gibson et al.,[36] who assume that reaction 3 is barrierless and exothermic. This assumption is inconsistent with the cross-section for reaction 3 in Figure 1 (and the rate coefficients in Figure 2), which increase with increasing kinetic energy. Because of experimental and theoretical results explained below, we report $D_0(Th^+{-}CH_2) \geq$ 4.54 ± 0.09 eV as a lower limit to the true BDE.

The calculated ground state of $ThCH_2^+$ is ^{2}A′ with a metal carbene geometry that has an agostic structure where one H is tilted toward the metal, essentially donating electron density from this CH bond into an empty d orbital on the metal. This agostic structure has been found to be characteristic of the early transition metals.[25,28,30,85] Geometrical parameters found here are similar to the structures reported by Di Santo et al.[41] and de Almeida and Duarte,[42] who also found a ^{2}A′ ground state. The CH_2 wagging motion passes through the symmetric $^2A_1$ state (a transition state having C_{2v} symmetry) lying only 0.05 eV higher in energy. A ^{2}A″ state is found 0.6 eV higher in energy, where the radical electron is moved from the a′-orbital composed primarily of the 7s-orbital to a 6d δ-like a″-orbital, and a ^{4}A″ state is 1.3 eV above the ground state. All other isomers, such as

DOI: 10.1021/acs.inorgchem.5b00137
Inorg. Chem. 2015, 54, 3584−3599

$HThCH^+$ and H_2ThC^+, are at least 1.3 eV above the ground state and can be found in Table S4 in the Supporting Information.

BDEs derived from the Seg. SDD theoretical calculations are listed in Table 3 and predict bond energies of 4.82−5.44 eV, not accounting yet for the spin−orbit contribution as discussed in the next section. CCSD(T)/KAP calculations indicate a BDE of 5.34 eV. The SDD and ANO basis sets yield similar results and can be found in Table S5. All levels of theory investigated here indicate that reaction 3 is exothermic when the associated theoretical value for $D_0(CH_2-H_2)$ is used. The range calculated here encompasses the theoretical value reported by Di Santo et al.[41] of 5.08 eV calculated at the B3LYP/SDD/6-311++G(d,p) level. They also report a theoretical value of 5.98 eV using PW91PW91/TZ2P employing a zero-order regular approximation (PW91/ZORA), but other BDEs determined using this method appear to overestimate bond strengths. All theoretical BDEs are consistent with the experimental lower limit and thus this comparison provides no definite quantitative information that allows evaluation of any theoretical method.

ThH^+. The threshold for reaction 4 is measured to be 2.38 ± 0.16 eV. Given $D_0(H_3C-H)$ = 4.48 ± 0.01 eV,[60] this suggests $D_0(Th^+-H)$ = 2.10 ± 0.16 eV. A similar result is obtained for the deuterated system, $D_0(Th^+-D)$ = 2.33 ± 0.11 eV. After accounting for zero-point energy differences (0.03 eV), the weighted average BDE is $D_0(Th^+-H)$ = 2.25 ± 0.18 eV. To the best of our knowledge, this represents the first experimental report of this bond energy.

For transition metal cations studied in our lab, BDEs measured using H_2 are 0.10−0.43 eV greater than those determined using CH_4 as a reactant.[22,23,25,27,28,30,53,69,70,86] In all cases, the difference is attributed to competition with the formation of the metal carbene because of a shared, common intermediate. Because reactions of M^+ with H_2 produce only one product, no competition exists that may delay the onset of reaction. For this reason, BDEs for metal hydrides measured using H_2 as the reaction partner are considered more reliable. Unpublished results[87] for the reaction of Th^+ with H_2 and D_2 determine that $D_0(Th^+-H)$ = 2.46 ± 0.07 eV, indicating that the average threshold for reaction 4 is delayed by 0.21 ± 0.19 eV. This observation is further substantiated by a phase space theory modeling of the competition between reactions 3 and 4, as described in greater detail in the Supporting Information and depicted in Figure S2. This model, which explicitly considers angular momentum effects, indicates that the threshold for reaction 4 is shifted by ∼0.3 eV, consistent with the more quantitative comparison above.

Di Santo and co-workers[41] calculated a $^3\Delta$ ground state for ThH^+ with a $^1\Sigma^+$ state very close in energy (0.02 eV) using B3LYP/SDD/6-311+G(p). Using a larger basis set for Th^+, we calculate similar results with a $^3\Delta$ ground state and low-lying excited states of $^1\Sigma^+$ (0.30 eV) and $^3\Pi$ (0.18 eV) at the B3LYP level of theory. CCSD(T) calculations reverse the order by placing the $^1\Sigma^+$ state 0.07 eV lower in energy than the $^3\Delta$ state and also indicate that the $^3\Pi$ is 0.37 eV higher in energy than the $^1\Sigma^+$. CCSD(T)/KAP calculations yield similar results, with the $^1\Sigma^+$ state 0.04 eV lower in energy than the $^3\Delta$ state. Bonding in ThH^+ occurs by combining the Th^+ (6d) and H (1s) electrons. The $^3\Delta$ correlates with the ^4F ($6d^27s$) state, where the unpaired electrons are found in essentially 6dδ and 7s atomic orbitals on the metal. Conversely, the $^1\Sigma^+$ state forms from the ^2D ($6d7s^2$) state of Th^+ with the 7s orbital filled. Given the mixed nature of the Th^+ ground level, formation of either state should be possible directly from the $J = {}^3/_2$ ground level. The $^3\Pi$, which places the 6d electron in a π orbital rather than a δ, should also form directly from the ground level.

Compared to experiment, Table 3, all levels of theory overbind ThH^+ by 0.3−0.5 eV, with the BHLYP value closest to the experimental value. Di Santo et al. report a similar BDE of 2.98 eV determined at the B3LYP/SDD/6-311++G(d,p) level and 3.49 eV using PW91/ZORA.[41] As for $ThCH_2^+$, the latter method appears to overestimate the bond strength significantly. Differences between the theoretical and experimental values for $D_0(Th^+-H)$ are attributable in part to spin−orbit splitting effects, as discussed in a following section.

$ThCH_3^+$. Because the $ThCH_3^+$ product dissociates readily to $ThCH^+$ at slightly higher energies, we determined the threshold for $ThCH_3^+$ production by analyzing the sum of these two product cross-sections. Using this procedure, the threshold for reaction 5 is 2.11 ± 0.15 eV, which corresponds to a bond energy for $D_0(Th^+-CH_3)$ of 2.37 ± 0.18 eV. Results from the CD_4 reaction lead to $D_0(Th^+-CD_3)$ = 2.44 ± 0.14 eV. After accounting for zero-point energy differences (0.04 eV), the weighted average BDE is $D_0(Th^+-CH_3)$ = 2.39 ± 0.22 eV. This value is likely a lower limit because, like ThH^+, $ThCH_3^+$ competes with reaction 3 through a shared intermediate such that the reaction 5 threshold may be delayed. Given that both experimental data and theoretical models (see Table 3) indicate that the BDEs for $ThCH_3^+$ and ThH^+ are similar, the delay in threshold onset for reaction 5 should be equivalent to the delay observed in reaction 4, 0.21 ± 0.19 eV. This conclusion is substantiated by the phase space theory modeling described in the Supporting Information, Figure S2. This model indicates that thresholds for both reactions 4 and 5 are shifted by comparable amounts that are consistent with a shift of 0.21 ± 0.19 eV. Therefore, a better estimate of the $ThCH_3^+$ BDE is $D_0(Th^+-CH_3)$ = 2.60 ± 0.30 eV. Previously, no theoretical or experimental report of the BDE for $ThCH_3^+$ has been made.

Similar to results for ThH^+, the DFT methods indicate that $ThCH_3^+$ has a ground state of ^3E with the unpaired electrons found in the 7s and 6d atomic orbitals and a low-lying level, $^1A_1$, only 0.06 eV above the ^3E for B3LYP. Additionally, a structural isomer, $HThCH_2^+$ ($^1A'$), is found nearly isoenergetic to the ^3E. CCSD(T) calculations place the $^1A_1$ and $^1A'$ states 0.22 and 0.01 eV, respectively, below the ^3E. CCSD(T)/KAP calculations place the $^1A_1$ and $^1A'$ states 0.18 and 0.19 eV lower in energy, respectively. Other structures and states investigated are listed in Table S4 but are found to be at least 2 eV higher in energy than $ThCH_3^+$ (^3E).

Theoretical BDEs listed in Table 3 for both the ^3E and $^1A_1$ states indicate that $D_0(Th^+-CH_3)$ and $D_0(Th^+-H)$ have similar magnitudes, with the former being stronger by 0.23−0.67 eV. Similar results are obtained using the SDD and ANO basis sets, Table S5. A direct comparison of the thresholds from reaction 4 and 5 in Table 1 suggests that $D_0(Th^+-CH_3)$ is 0.27 ± 0.22 eV larger than $D_0(Th^+-H)$ and that $D_0(Th^+-CD_3)$ is 0.12 ± 0.14 eV larger than $D_0(Th^+-D)$, with a weighted average (after ZPE corrections) of 0.15 ± 0.12 eV. This is comparable to results for the transition metal congeners, Zr^+,[15,53] and Hf^+,[25,69] where MCH_3^+ and MH^+ BDEs are similar in strength, and to Ti^+,[88] where the BDE for $TiCH_3^+$ is stronger than that for TiH^+ by 0.2 ± 0.2 eV. Similar to the results for ThH^+, theory overbinds by 0.4−0.9 eV, again, in part because of spin−orbit effects discussed below.

$ThCH^+$. The threshold for reaction 6 is 3.08 ± 0.17 and 2.98 ± 0.06 eV for the deuterated analogue, Table 1. The correlation

DOI: 10.1021/acs.inorgchem.5b00137
Inorg. Chem. 2015, 54, 3584−3599

between the decline in the cross-section for $ThCH_3^+$ at the apparent onset for the formation of $ThCH^+$ indicates that this product is formed by the dehydrogenation of $ThCH_3^+$. Thus, we combine these thresholds with $D_0(H_2C-H_2) + D_0(HC-H) = 9.07 \pm 0.02$ eV[60] and the value of its deuterated counterpart to obtain BDEs of $D_0(Th^+-CH) = 5.99 \pm 0.20$ eV and $D_0(Th^+-CD) = 6.27 \pm 0.09$ eV. After accounting for differences in the zero-point energy (0.03 eV), the weighted average is $D_0(Th^+-CH) = 6.19 \pm 0.16$ eV.

The ground-state structure of $ThCH^+$ identified by theory is a linear methylidyne having a $^1\Sigma^+$ ground state. Several geometries including bent and linear insertion ($HThC^+$) geometries were also investigated, but these are all found to be at least 2.2 eV higher in energy, as detailed in Table S4.

Theoretical predictions of $D_0(Th^+-CH)$ range from 0.4 eV too high (B3PW91) to 0.6 eV too low in energy (BHLYP) with the values derived from B3LYP and CCSD(T) (Seg. SDD and KAP) within experimental uncertainty. Benchmark studies by Zhang and Schwarz[89] indicate that although BHLYP performs well for MCH_3^+ species it performs poorly for other MCH_x^+ systems. Studies from our group have also observed similar poor performance by BHLYP for studies involving higher bond order third-row transition metal species,[23,25−28,30] indicating that BHLYP is an inappropriate choice of level of theory for the study of species with bond orders higher than 1.

$ThCH_4^+$. The threshold for reaction 7 obtained using eq 1 is 0.46 ± 0.05 eV, which should equal $D_0(Th^+-CH_4)$, as discussed below. Previous work[90,91] in our lab has indicated that collisionally excited association complexes may have a sufficiently long lifetime such that dissociation does not occur within the experimental time frame of 1×10^{-4} s. In such cases, the apparent threshold is higher than the true bond energy because of a kinetic shift in the threshold.[91,92] Therefore, the cross-section for reaction 7 was also modeled using a modified version of eq 1 that incorporates RRKM rate theory[93,94] to account for any possible kinetic shift. This model, which has been thoroughly explained elsewhere,[91,92] yields a threshold of 0.47 ± 0.05 eV, indicating that there is no significant kinetic shift, consistent with the simplicity of this system.

The ground state of $Th^+(CH_4)$ is ^2A with a calculated structure that is nonsymmetrical as Th^+ binds to CH_4 such that the bond lengths $r(Th-H)$ of the three closest H atoms are 2.71, 2.70, and 2.66 Å. The methane is largely unperturbed, consistent with the formation of an electrostatic bond. Both Di Santo et al.[41] and de Almeida and Duarte[42] also report a ^2A structure for the ground state of $Th^+(CH_4)$. A more symmetrical $^2A'$ state is also found 0.1−0.2 eV higher in energy. A $^4A''$ state lies 0.06−0.22 eV higher in energy than the ^2A state, Table S4.

The theoretical BDEs of the $Th^+(CH_4)$ (^2A) state relative to Th^+ (^2D, $6d7s^2$) + CH_4 range from 0.33−0.64 eV, Table 3, where B3LYP and B3PW91 overestimate the bond strength and BHLYP and CCSD(T) are too low in energy. Results using the SDD and ANO basis sets are similar with the exception of the BHLYP/SDD and CCSD(T)/SDD values, which underestimate the bond strength by ~0.2 eV, Table S5. CCSD(T)/KAP results place the BDE slightly outside of experimental uncertainty. Di Santo et al.[41] report theoretical BDEs of 0.32 and 1.05 eV using B3LYP/SDD/6-311++G(d,p) and PW91/ZORA, respectively. Again, PW91/ZORA appears to significantly overestimate the BDE, and the B3LYP value is somewhat low. Theoretical BDEs of 0.47 and 0.44 eV calculated by B3PW91/DZP/6-311++G(d,p) and B3LYP/DZP/6-311++G(d,p), respectively, can also be inferred from de Almeida and Duarte's potential energy surface for reaction 3.[42] These latter values are in good agreement with the experimental and theoretical values determined here.

As discussed more thoroughly below, the lowest energy structure for $ThCH_4^+$ is not $Th^+(CH_4)$ but rather the inserted $HThCH_3^+$. Theoretical BDEs for this inserted species losing CH_4 range from 1.47−2.00 eV, well above the experimental value. Given the agreement between theoretical and experimental BDEs for $Th^+(CH_4)$, it can be concluded that $ThCH_4^+$ complex formed in our experiment is $Th^+(CH_4)$. By extension, the failure to generate $HThCH_3^+$ in the flow tube source suggests that there must be a barrier in excess of thermal energies when Th^+ interacts with methane. The presence of this barrier will be explored in greater detail below.

Doublet Potential Energy Surface for $Th^+ + CH_4$ Reaction. The potential energy surfaces for reactions 3−5 were calculated using several basis sets for Th^+. The PES at the CCSD(T)/Seg. SDD/6-311++G(3df,3p)//B3LYP/SDD/6-311++G(d,p) level of theory appears to reproduce the experimental data most accurately and is presented in Figure 4, with structures in Figure 5. Geometrical parameters can be found in Table S6 in the Supporting Information. The energies of each intermediate and transition state (TS) as well as values from additional levels of theory are in Table 4. Energies from the SDD and ANO basis sets are listed in Table S7 in the Supporting Information. Most energies in Figure 4 and Table 4 are relative to the Th^+ (^2D, $6d7s^2$) + CH_4 reactants except where explicitly noted otherwise. As discussed in detail below, accounting for spin−orbit interactions is critical when comparing the PESs to experimentally measured values. Thus, the solid lines in Figure 4 denote surfaces with spin−orbit energy explicitly accounted for and the dotted lines represent the uncorrected surfaces. Geometries and electronic states of all of the intermediates and transition states are similar to those reported by Di Santo et al. (B3LYP)[41] and de Almeida and Duarte (B3PW91),[42] and their calculated values are included in Table 4. (Note that these are referenced to different ground-state reactants.) When compared to the present calculations using the same level of theory and the same reactant state, the

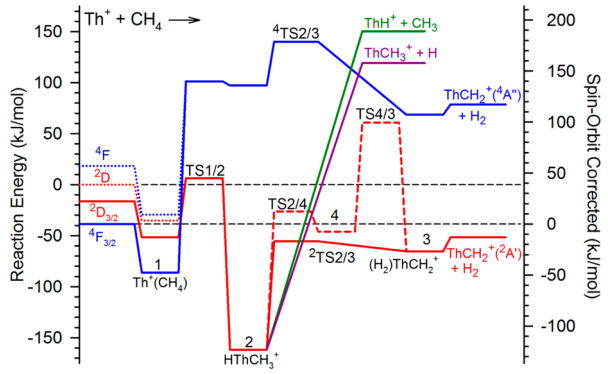

Figure 4. Potential energy surface for the reaction of methane with thorium cation calculated at the CCSD(T)/Seg. SDD/6-311++G(3df,3p)//B3LYP/SDD/6-311++G(d,p) level of theory. The full lines show spin−orbit corrected surfaces relative to Th^+ ($^4F_{3/2}$) + CH_4 and are indicated by the axis on the right. Dotted lines and full line past TS1/2 show uncorrected surfaces relative to Th^+ (^2D) + CH_4 and are indicated by the axis on the left. Doublet surface is in red, and quartet, blue.

DOI: 10.1021/acs.inorgchem.5b00137
Inorg. Chem. 2015, 54, 3584−3599

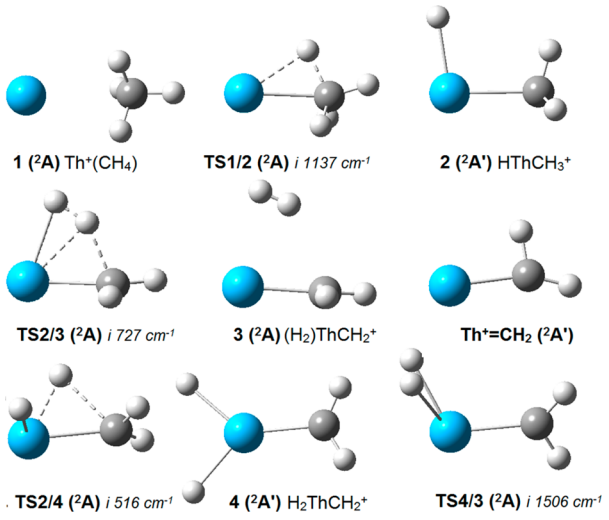

Figure 5. Geometrical structures of each doublet spin intermediate and transition state in Figure 4. All structures were optimized using the B3LYP/SDD/6-311++G(d,p) approach.

mean absolute deviations in all energies are about 11 and 12 kJ/mol, respectively. Similar to the reaction coordinate published by Di Santo et al.,[41] before spin−orbit interactions are included, the reaction appears to evolve entirely along the doublet surface. This contrasts with B3PW91 calculations of de Almeida and Duarte, where they observe a crossing between the reactants' ground quartet surface and the doublet surface near the first intermediate because their calculations place Th^+ (^4F) below Th^+ (^2D).[42] No such crossing point was observed at any level of theory studied here, although the doublet and quartet thorium−methane adducts are close in energy at the B3PW91, BHLYP, and CCSD(T) levels of theory, Table 4.

The first intermediate (^{2}**1**) is the association complex, $Th^+(CH_4)$, where the methane is largely unperturbed. ^{2}**1** (^{2}A) lies 31−62 kJ/mol lower in energy than the ground-state reactants, which is consistent with the CID threshold of 45.3 ± 4.8 kJ/mol in reaction 7 (Figure 3). It is worth noting that ^{2}**1** is the only intermediate that shows spin contamination, $s(s+1)$ = 1.35−1.69 in the present calculations, of a similar magnitude to that of the Th^+ separated atom. This spin contamination probably arises from the proximity (in energy) of the quartet intermediate. This intermediate has similar geometric properties to the doublet analogue and is only 6−22 kJ/mol higher in energy.

The first transition state (^{2}**TS1/2**) connects ^{2}**1** with the global minimum ^{2}**2**, $HThCH_3^+$, the thorium hydrido methyl cation intermediate. The $r(Th^+-C)$ bond decreases from 2.78 Å in ^{2}**1** to 2.29 Å in ^{2}**TS1/2**, a single C−H bond elongates from 1.10 to 1.37 Å, and the H moves closer to the metal center. ^{2}**TS1/2** (^{2}A) lies 6 and 26 kJ/mol above the reactants according to CCSD(T) and BHLYP calculations, respectively, whereas B3LYP and B3PW91 indicate that ^{2}**TS1/2** lies below the reactants by 17 and 35 kJ/mol, all referenced to the Th^+ (^{2}D) + CH_4 asymptote. Di Santo and co-workers previously reported the presence of a 5 kJ/mol barrier in similar B3LYP calculations;[41] however, their reported potential energy surface was referenced to the Th^+ (^{2}F, 5f7s^2) state that is the ground state for B3LYP and B3PW91 calculations but is 18−56 kJ/mol (Table 2) higher in energy for the other levels of theory and 42 kJ/mol higher experimentally. The use of the ^{2}F state as the reference in our surface would lead to a barrier of 2 kJ/mol for the surface calculated using B3LYP/Seg. SDD/6-311++G-(3df,3p), similar to the result of Di Santo and co-workers. No barrier is observed in the results of de Almeida and Duarte, who place the ^{2}TS1/2 transition state 7−25 kJ/mol below the ^{2}D

Table 4. Single-Point Energies (kJ/mol) Relative to the Th^+ + CH_4 Reactants without and (with) Spin−Orbit Corrections[a]

		this work				literature	
species	state	CCSD(T)	B3LYP	B3PW91	BHLYP	B3LYP[b]	B3PW91[c]
$Th^+ + CH_4$	$^2D + {}^1A_{1g}$	0.0 (22.2)	0.0 (22.2)	0.0 (22.2)	0.0 (22.2)	0.0 (^{2}F)	6.8
	$^4F + {}^1A_{1g}$	18.3 (0.0)	17.4 (0.0)	1.0 (0.0)	17.4 (0.0)	24.4	0.0
$Th^+(CH_4)$ (1)	^2A	−35.2 (−13.0)	−53.7 (−31.5)	−61.7 (−39.5)	−31.5 (−9.3)	−30.9	−45.0
	$^4A''$	−29.4 (−47.5)	−32.0 (−49.4)	−54.1 (−55.4)	−24.4 (−41.8)	−10.1	−27.7
TS1/2[d]	^2A	6.2 (44.8)	−17.1 (21.5)	−35.0 (3.6)	26.4 (65.0)	4.8	−18.3
	^4A	101.2 (139.8)	72.2	58.8	85.2	97.8	94.6
$HThCH_3^+$ (2)	$^2A'$	−161.8 (−123.2)	−188.7	−202.3	−163.7	−168.0	−186.0
	$^4A'$	97.2 (135.8)	61.1	48.9	81.2	79.3	62.1
TS2/3	^2A	−55.5 (−16.9)	−75.3	−101.2	−25.6	−52.7	−81.4
	^4A	140.1 (178.7)	109.5	82.5	143.3		101.5
TS2/4	^2A	−26.2 (12.4)	−64.0	−79.4	−27.0	−43.1	−62.1
$H_2ThCH_2^+$ (4)	$^2A'$	−46.0 (−7.4)	−84.4	−94.8	−61.7	−62.7	
TS4/3	^2A	60.8 (99.4)	9.4	−12.8	61.0	30.4	6.0
$(H_2)ThCH_2^+$ (3)	^2A	−65.4 (−26.8)	−79.0	−98.4	−35.5	−57.3	−81.8
	^4A	68.5 (107.1)	41.2	21.8	65.0	62.6	39.4
$ThCH_2^+ + H_2$	$^2A' + {}^1\Sigma_g^+$	−51.6 (−13.0)	−63.9 (−25.3)	−77.2 (−38.6)	−22.2 (16.4)	−42.4	−59.8
	$^4A'' + {}^1\Sigma_g^+$	78.6 (117.2)	53.4	39.2	74.0	68.9	58.6

[a]Structures were optimized and vibrational frequencies calculated using B3LYP/SDD/6-311++G(d,p). Single-point energies were calculated at the respective level of theory with Seg. SDD/6-311++G(3df,3p) and zero-point corrected (scaled by 0.989). Values in parentheses are relative to Th^+ ($^4F_{3/2}$) + CH_4 and corrected by the empirical difference between the ^{2}D state averaged over all spin−orbit levels and the $^4F_{3/2}$ level, 38.6 kJ/mol, except for **1** where the well depth remains constant relative to its asymptote; see the text. Note that the spin−orbit corrected reactant asymptotes are fixed at their empirical energy difference. [b]Ref 41. [c]Ref 42.

DOI: 10.1021/acs.inorgchem.5b00137
Inorg. Chem. 2015, 54, 3584−3599

asymptote and 15−18 kJ/mol below the ^{4}F ground asymptote.[42]

The ground state of $HThCH_3^+$, ^{2}**2**, where the metal is inserted into one of the C−H bonds, lies 162−202 kJ/mol below ground-state reactants. It has a ^{2}A′ ground state with r(Th−H) = 2.00 Å and r(Th−CH_3) = 2.32 Å bond lengths. These are comparable to r(Th−H) for ThH^+ of 1.99 Å and r(Th−CH_3) for $ThCH_3^+$ of 2.31 Å, consistent with the formation of single covalent bonds between the Th cation (having three valence electrons) and both ligands, which necessitates having the doublet low-spin. (Thus, the quartet state of this species can no longer form two covalent bonds, leading to the much higher energy.)

^{2}**TS2/3** has a ^{2}A ground state and lies 26−101 kJ/mol below the reactants in energy. ^{2}**TS2/3** is a four-centered transition state in which another C−H bond elongates from 1.10 to 1.71 Å as this second H is transferred from the C to the H ligand. Thus, the Th^+−H bond in ^{2}**2** lengthens, consistent with the Th^+−H covalent bond beginning to break as the H−H bond forms. This leads to ^{2}**3** (^{2}A), a thorium carbene cation−dihydrogen association complex, $(H_2)ThCH_2^+$, which lies 35−98 kJ/mol lower than the reactants. Loss of H_2 from ^{2}**3** requires only 13−21 kJ/mol and leads to the $ThCH_2^+$ (^{2}A′) + H_2 products. Overall, the dehydrogenation reaction is calculated to be exothermic by 22−77 kJ/mol along the doublet surface.

An alternative pathway for dehydrogenation is to proceed through ^{2}**TS2/4**, which forms when a second hydrogen is transferred to the metal center to form ^{2}**4**, a dihydride carbene cation, $H_2ThCH_2^+$. In this case, both r(Th−H) bonds have lengths of 2.01 Å, consistent with covalent bonds, and the ∠HThH angle (100.7°) is much larger than ∠HThH (25.3°) in ^{2}**TS2/3**. Furthermore, r(Th−C) = 2.32 Å in ^{2}**4** is longer than r(Th−C) = 2.11 Å in ^{2}**TS2/3**, considerably longer than r(Th−C) = 2.04 Å in the $ThCH_2^+$ product, and equivalent to r(Th−C) = 2.31 Å in $ThCH_3^+$, showing that the Th−C bond in ^{2}**4** no longer has double-bond character. ^{2}**4** has a ^{2}A′ ground state that converts to ^{2}**3** through ^{2}**TS4/3** (^{2}A) by rotating the hydrogens located on the Th^+ together. As this pathway is considerably higher in energy (by 85−116 kJ/mol) than passing through ^{2}**TS2/3**, it is unlikely to be influential experimentally.

Quartet Potential Energy Surface for Th^+ + CH_4 Reaction. The quartet surface presented here is energetically less favorable than the doublet surface at all points along the surface for all levels of theory investigated, Table 4. The structures of all intermediates and transition states are similar to their analogous doublet structures and are pictured in Figure S3 in the Supporting Information. The surface originates from Th^+ (^{4}F, 6$d^2$7s) + CH_4, which is 2−18 kJ/mol higher in energy than Th^+ (^{2}D, 6d7s^2) + CH_4. The $Th^+(CH_4)$ association complex of CH_4 with Th^+, where the methane is largely unperturbed, ^{4}**1**, is 6−22 kJ/mol higher in energy than ^{2}**1** with r(Th−C) increased by 0.12 Å. The surface is repulsive as it moves through ^{4}**TS1/2** to ^{4}**2** and r(Th−C) decreases from 2.90 to 2.86 Å. ^{4}**TS1/2** lies 59−95 kJ/mol higher in energy than ^{2}**TS1/2**, and ^{4}**2** lies 245−259 kJ/mol higher in energy than ^{2}**2**, with r(Th−H) and r(Th−C) being 0.05 and 0.37 Å longer, respectively. Thus, the higher spin state means that the $HTh-CH_3$ bond is no longer a covalent single bond, greatly increasing the energy of this species. ^{4}**2** is connected to ^{4}**3** by ^{4}**TS2/3**, which is 169−196 kJ/mol higher in energy than ^{2}**TS2/3**. ^{4}**3** is a thorium carbene cation−dihydrogen association complex that is 100−134 kJ/mol higher in energy than ^{2}**3**. Similar to the doublet complex, loss of H_2 requires only 9−17 kJ/mol to dissociate to the products, $ThCH_2^+$ (^{4}A″) + H_2. Overall, the dehydrogenation reaction along this pathway is 39−79 kJ/mol endothermic compared to the ^{2}D ground-state reactants and 96−130 kJ/mol above the $ThCH_2^+$ (^{2}A′) + H_2 products. Notably, r(Th−C) of $ThCH_2^+$ (^{4}A″) is 2.32 Å, 0.27 Å longer than $ThCH_2^+$ (^{2}A′) and similar to $ThCH_3^+$, where r(Th−C) = 2.31 Å. Thus, the high-spin state of $ThCH_2^+$ (^{4}A″) no longer allows a Th−C covalent double bond.

DISCUSSION

Spin−Orbit Corrections to Theoretical BDEs. The present theoretical calculations correspond to the average energy over all spin−orbit levels in a given state; however, the experimental results presented here should correspond to the energies of the lowest spin−orbit states. For Th^+, this effect is quite large, thereby accounting for much of the deviation between theoretical and experimental BDEs. In order to make a better comparison between theory and experiment, it is necessary to explicitly estimate the spin−orbit energies. For dissociation of Th^+−L bonds, the experimental asymptote for Th^+ + L lies below the theoretical asymptote such that the theoretical BDE should be lowered by the average excitation energy of Th^+ and the ligands (where the spin−orbit correction for the latter is negligible here) and raised by the spin−orbit splitting of the ground state of ThL^+. Th^+ is an interesting case, where the ground state averaged over all spin−orbit levels is ^{2}D, but the ground level is $^4F_{3/2}$. The estimation of the spin−orbit effects of the asymptote can be done in two ways. The first is to consider that the spin state and bonding of the molecules listed in Table 3 (except ThH^+ ($^1\Sigma^+$), $ThCH_3^+$ ($^1A_1$), and $ThCH_4^+$ (^{2}A)) necessitate that the molecules are diabatically associated with the Th^+ (^{4}F) + L asymptote. Thus, to include the spin−orbit effects of the Th^+ + L asymptote, the theoretically calculated BDE for dissociation to Th^+ (^{4}F) + L (rather than for dissociation to the ^{2}D state as listed in Table 3) is corrected to the Th^+ ($^4F_{3/2}$) + L asymptote by the empirical difference in energy of the ^{4}F state averaged over all spin−orbit levels and the $^4F_{3/2}$ level, 3729.960 cm^{-1} = −0.46 eV, Table S1. When necessary, the BDE is also corrected by the spin−orbit splitting of the respective ThL^+ molecule, as estimated below. Utilizing this method yields mean absolute deviations (MADs) of 0.31−0.41 eV compared to experimental values excluding $ThCH_2^+$. The second method is to correct directly from the Th^+ (^{2}D) + L asymptote to the Th^+ ($^4F_{3/2}$) + L asymptote by the difference between the $^4F_{3/2}$ level and the ^{2}D state averaged over all spin−orbit states. Empirically, the $^4F_{3/2}$ lies 3211.991 cm^{-1} = 0.40 eV below the ^{2}D state, Table S1. Utilizing this method yields MADs of 0.27−0.38 eV, Table 3, indicating that this method provides slightly more reliable predictions, which is why the latter method is used here.

It should be noted that this semiempirical approach to estimating spin−orbit effects is only a first-order approximation, as second-order effects associated with coupling with other states is possible in some instances (mentioned specifically below). An estimation of these effects is beyond the scope of the present approach, such that we assume such second-order perturbations are negligible, which may lead to (potentially significant) errors in the estimated stabilization energies. We also note that rigorous theoretical methods designed to treat spin−orbit interactions tend to underestimate the experimentally observed couplings.[95]

DOI: 10.1021/acs.inorgchem.5b00137
Inorg. Chem. 2015, 54, 3584−3599

$ThCH_2^+$ has a $^2A'$ ground state and hence has no spin−orbit splitting. Second-order interactions of this state with the $^2A''$ and $^4A''$ states may occur, but these interactions are assumed to be negligible because these states are much higher in energy, Table S4. Thus, spin−orbit corrections to $D_0(Th^+-CH_2)$ involve only the average excitation energy of −0.40 eV from the Th^+ (^2D) + CH_2 asymptote. After including this spin−orbit energy correction, the theoretical BDEs for $ThCH_2^+$ are 4.42 (BHLYP) and 4.74−5.04 eV, Table 3, such that reaction 3 is endothermic by 0.17 for BHLYP, whereas the other levels predict the reaction will be exothermic by 0.13−0.40 eV (Table 4). Note that the BHLYP result (which is suspect for this multiply bonded species) is potentially consistent with the threshold experimentally measured for reaction 3; however, at all levels of theory, the barrier at ^{2}**TS1/2** in the reaction coordinate (Figure 4) lies 42−58 kJ/mol above the product asymptote. Thus, theory indicates that the threshold must correspond to the barrier at ^{2}**TS1/2**. Therefore, our experimental value of $D_0(Th^+-CH_2)$ can be reported only as a lower limit to the true BDE, although CCSD(T), B3LYP, and B3PW91 levels all indicate that the bond is not that much stronger. Nevertheless, comparison of experimental and theoretical results with and without explicitly accounting for spin−orbit effects is inexact.

$ThCH^+$ has a $^1\Sigma^+$ ground state, which has no spin−orbit splitting, so, like $ThCH_2^+$, the only spin−orbit correction to the BDE needed is that from the Th^+ (^2D) + CH asymptote. Here, second-order spin−orbit interactions are assumed to be negligible because the appropriate excited states with which the $^1\Sigma^+$ ground state can interact are much higher in energy, Table S4. When this spin−orbit correction is included, the theoretical BDEs are 5.17 (BHLYP) and 5.64−6.21 eV, Table 3, where the latter values are in reasonable agreement with the experimental value of 6.19 ± 0.16 eV. BHLYP underestimates the BDE by the most (∼1 eV), which, as noted above, is typical of BHLYP calculations for multiply bonded species. Excluding the BHLYP results, the average deviation between theory and experiment when spin−orbit corrections are included is 0.32 ± 0.27 eV, which is comparable to the average deviation without including spin−orbit corrections (0.19 ± 0.20 eV). Thus, the applied correction does little to improve (or harm) the theoretical BDEs in this case. CCSD(T)/KAP calculations are similar to both the uncorrected and corrected BDEs, being slightly outside of experimental uncertainty.

Previous work has successfully estimated the spin−orbit splitting for third-row transition metal molecules[30,96−98] by using

$$E^{SO} = \Lambda M_S A \quad (8)$$

where A is the spin−orbit splitting constant, Λ is the orbital angular momentum quantum number, and M_S is the spin quantum number associated with a particular level $\Omega = \Lambda + M_S$.[99] E^{SO} is also equal to the summation $\sum a_i l_i \cdot s_i$, where $l_i \cdot s_i$ is the dot product of the orbital angular momentum and the spin of electron i and a_i is the spin−orbit parameter, which can be represented by the atomic spin−orbit parameter for the 6d electrons of thorium $\zeta_{6d}(Th)$. To the best of our knowledge, this constant has not been determined experimentally, but we estimate that $\zeta_{6d}(Th) = 1458\ cm^{-1}$, as explained in the Supporting Information.

The $^3\Delta$ state of ThH^+ splits into $^3\Delta_1$, $^3\Delta_2$, and $^3\Delta_3$ levels where $^3\Delta_1$, with $\Lambda = 2$ and $M_S = -1$, is the ground level. Using eq 8 and our estimated value of $\zeta_{6d}(Th)$, this ground level lies relative to the spin−orbit average value by $E^{SO} = 2\ (-1)A = -\zeta_{6d}(Th) = -1458\ cm^{-1} = -0.18$ eV so that $A = 729\ cm^{-1}$. The splitting for $^3\Delta_2$ is $E^{SO} = 2\ (0)A = 0.0$ eV, and the $^3\Delta_3$ level is destabilized by $E^{SO} = 2\ (1)A = 0.18$ eV from the unperturbed state. Thus, the theoretical BDEs for ThH^+ ($^3\Delta$) relative to Th^+ (^2D) should be decreased by 0.40 eV, the difference between the average ^2D and $^4F_{3/2}$ level for Th^+, and increased by 0.18 eV to account for the splitting in the $^3\Delta_1$ state. Doing so yields BDEs of 2.57−2.96 eV for the ThH^+ ($^3\Delta_1$) state, Table 3. In general, inclusion of spin−orbit corrections improves the agreement between the theoretical BDEs for ThH^+ and the experimental value, with the BHLYP result within experimental uncertainty, CCSD(T)/Seg. SDD nearly so, and the other methods slightly higher.

The $^1\Sigma^+$ state of ThH^+ has no spin−orbit splitting, so BDEs need to be corrected only by the difference in energy between the average ^2D state and the $^4F_{3/2}$ level. Applying this correction, BDEs for the $^1\Sigma^+$ state are 2.26−2.47 and 2.55 eV for CCSD(T)/KAP. As noted above, the predicted ground state for ThH^+ is $^3\Delta$ for all methods except CCSD(T), such that these BDEs should not correspond to the experimentally measured value. In the CCSD(T) case, a $^1\Sigma^+$ ground state lying 0.07 eV below the $^3\Delta$ is predicted, but after including spin−orbit effects, the $^3\Delta_1$ lies 0.11 eV below the $^1\Sigma^+$. CCSD(T)/KAP calculations indicate that the $^3\Delta_1$ lies 0.14 eV below the $^1\Sigma^+$. Additionally, eq 8 indicates that the stabilization of the $^3\Pi_0$ level is only 0.09 eV such that the $^3\Delta_1$ is predicted to be the ground level at all levels of theory. The results using the ANO basis set are similar, whereas the SDD basis set indicates that the $^1\Sigma^+$ and $^3\Delta_1$ are isoenergetic, Table S5. Further complicating the assignment of the ground level is the second-order spin−orbit interaction of the $^3\Delta_1$ level with the $^3\Pi_1$ and of the $^1\Sigma^+$ with the $^3\Pi_0$ level. In these cases, the interactions should stabilize both the $^3\Delta_1$ and $^1\Sigma^+$ levels, but we make no attempt to quantify this effect. Because both the $^3\Delta$ and $^1\Sigma^+$ states can be formed directly from the (^4F,^2D) mixed ground level of Th^+, the mixed results here preclude a confident determination of the true ThH^+ ground electronic state.

The calculated ground state of $ThCH_3^+$ is ^3E (DFT) or $^1A_1$ (CCSD(T)). Like ThH^+ ($^3\Delta$), the unpaired electrons in the triplet state are d^1s^1, where the d-electron is found in a δ-like orbital. As an approximation to the spin−orbit splitting for the ^3E state, we assume that the splitting is similar to that for ThH^+ ($^3\Delta$). The $^1A_1$ state has no spin−orbit corrections. Unlike ThH^+, after inclusion of spin−orbit effects, the $^1A_1$ still lies below the ^3E for CCSD(T) and the states are isoenergetic for CCSD(T)/KAP. After applying the spin−orbit corrections, the theoretical BDEs are 2.76−3.32 eV for the ^3E and 2.56−3.00 eV for the $^1A_1$ (3.22 eV for CCSD(T)/KAP), Table 3, improving the agreement with the experimental value of $D_0(Th^+-CH_3) = 2.60 \pm 0.30$ eV. Here, the BHLYP value for the ^3E is within experimental uncertainty of the experimental BDE, and the CCSD(T)/Seg. SDD value for the $^1A_1$ is just outside the experimental range.

The calculated ground state of $Th^+(CH_4)$ is ^2A, where the CH_4 is loosely bound and largely unperturbed. Because bonding results from electrostatic interactions between Th^+ and CH_4, a zero-order approximation of the spin−orbit splitting of this molecule assumes it is very similar to that found on the atomic metal center when unperturbed. Thus, we make no spin−orbit corrections to the theoretical BDEs for this species; however, because the $^4F_{3/2}$ level lies 0.23 eV (1859.938

DOI: 10.1021/acs.inorgchem.5b00137
Inorg. Chem. 2015, 54, 3584−3599

cm^{-1}) below the $^2D_{3/2}$ level (Table S1) and the calculated BDEs for ^{2}1 and ^{4}1 are comparable (within 0.13 eV, Table 4), the ground state of $Th^+(CH_4)$ becomes the $^4A''$ at all levels of theory. The theoretical BDEs for this state are 0.43−0.57 and 0.51 eV for CCSD(T)/KAP, in very good agreement with the experimental value, Table 3.

This first-order approximation to the true spin−orbit interaction in $Th^+(CH_4)$ cannot be rigorously correct because the degenerate d-orbitals of the nonperturbed Th^+ will be split by interaction with CH_4, which can be thought about in terms of a simple donor−acceptor model. When CH_4 is brought into close proximity, it donates electron density into the d_{z2}-orbital. This interaction of the σ-like orbitals of the Th^+ and CH_4 leads to a pair of bonding and antibonding orbitals, such that the d_{z2}-orbital is pushed up in energy. Simultaneously, the δ−like orbitals on Th^+ are largely noninteractive with CH_4, whereas the π-like d-orbitals interact with antibonding orbitals on CH_4 stabilizing these orbitals. This analysis agrees with the results of our calculations on $Th^+(CH_4)$ (^2A), where the unpaired electron is located in a π-like 6d-orbital located on Th^+ and with those for $Th^+(CH_4)$ ($^4A''$) where the unpaired electrons are in the 7s-orbital and two π-like 6d-orbitals. Thus, to a first approximation, the theoretical results naturally account for the orbital occupation preference, but a quantitative account of how these interactions change the first-order spin−orbit correction applied above is not attempted here. The approximation made here should be reasonable as long as the splitting of the degenerate 6d-orbital energies resulting from the ligand is smaller than the spin−orbit splitting of the free ion. This assumption appears to be reasonable because of a favorable comparison to the experimental value for the $Th^+(CH_4)$ well depth.

Bonding in $ThCH_x^+$. Figure 6 shows a comparison of the $D_0(Th^+-CH_x)$ values with their organic analogues, $D_0(H_xC-CH_x)$. Such a plot is a useful means of experimentally determining bond order and has proven to be useful for many transition metal systems.[15,22,25,28,30] The solid line represents the least-squares linear regression constrained to pass through the origin. In order to ascertain a more accurate trend, $D_0(Th^+-H)$ = 2.46 ± 0.07 eV from the reaction of Th^+ with H_2 and the adjusted value for $D_0(Th^+-CH_3)$ are used.[87] Notably, there is no meaningful change in the trend line when $D_0(Th^+-CH_2)$, which is a lower limit, is excluded from the fit. This suggests that the true value of $D_0(Th^+-CH_2)$ is unlikely to be much higher than the limit, consistent with theory. The good correlation of the plot clearly indicates that Th^+-H and Th^+-CH_3 are single bonds, $Th^+=CH_2$ is a double bond, and $Th^+\equiv CH$ is a triple bond. These assignments are fully consistent with the quantum chemical calculations described above.

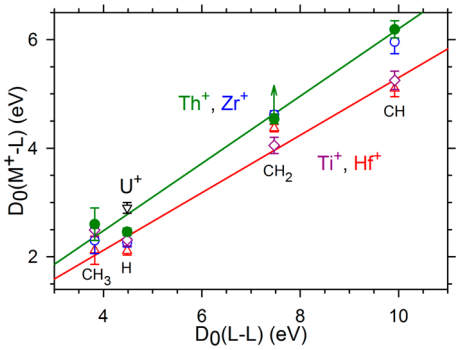

Figure 6. Bond energy−bond order comparison of M^+-L for M^+ = Th^+ (green), Zr^+ (blue), Hf^+ (red), Ti^+ (purple), and U^+ (black) by plotting $D_0(M^+-L)$ versus $D_0(L-L)$.

It is also interesting to compare these BDEs with those of several related metals. Unfortunately, comparable experimental data for other actinides do not exist with the exception of $D_0(U^+-H)$ = 2.9 ± 0.1 eV.[34] However, because Th^+ does not occupy the 5f orbitals in its ground state, a better comparison might be to transition metals with three valence electrons: Hf^+ (^2D, $5d6s^2$), Zr^+ (^4F, $4d^25s$), and Ti^+ (^4F, $3d^24s$). In this regard, it is worth noting the similarities of Th^+ with Hf^+, where experiment and theory both assign a ^2D ($5d6s^2$) ground state.[25,55,69] In calculations of the Hf^+ (^2D) state, the observed spin contamination, $s(s+1) \sim 1.2$, is comparable to that of the Th^+ system.[25] The BDEs for these metals are compared to those for Th^+ in Table 5 and Figure 6. The slope of the trend line for Th^+, m = 0.62, is very similar to that of Zr^+, m = 0.60, and systematically higher than those observed for Hf^+, m = 0.53, and Ti^+, m = 0.54. Thus, the relative BDEs are $Ti^+ \approx Hf^+ < Zr^+ \approx Th^+$. Typically, BDEs increase moving down the periodic table because of the lanthanide contraction,[22,23,26,27,89] leading to an expected trend in BDEs of $Ti^+ < Zr^+ < Hf^+ < Th^+$. The lower BDEs of Hf^+ (^2D, $5d6s^2$) have previously been explained by the filled 6s orbital, which inhibits bond formation,[25] compared to the open d-shell configurations of Ti^+ (^4F, $3d^24s$) and Zr^+ (^4F, $4d^25s$). Likewise, the partial ^2D character of the ground $J = {}^3/_2$ level may suppress the BDEs of Th^+ somewhat.

The individual trends for each bond type indicate that for the singly bonded M^+-H and M^+-CH_3 the BDE trend is $Hf^+ < Zr^+ < Ti^+ < Th^+$, whereas the multiply bonded species, M^+-CH_2 and M^+-CH, have bonds that follow the order $Ti^+ < Hf^+ < Zr^+ \approx Th^+$ and $Hf^+ < Ti^+ < Zr^+ < Th^+$, respectively. Presumably, some of these variations are associated with the strength of the π-bonds, which can vary through the periodic table because of overlap differences as the size of the d orbitals on the metal changes. Despite some deviation from the expected trend for the smaller metal cations, Th^+ BDEs are

Table 5. Comparison of BDEs (eV) for Th^+ and Transition Metal Congeners

metal	slope[a]	$D_0(M^+-CH_3)$	$D_0(M^+-H)$	$D_0(M^+-CH_2)$	$D_0(M^+-CH)$
Ti[b]	0.54	2.49 ± 0.12	2.31 ± 0.11	4.05 ± 0.15	5.25 ± 0.17
Zr	0.60	2.30 ± 0.24[c]	2.26 ± 0.08[d]	4.62 ± 0.07[c]	5.96 ± 0.22[c]
Hf	0.53	2.12 ± 0.27[e]	2.11 ± 0.08[f]	4.37 ± 0.07[e]	5.10 ± 0.15[e]
Th	0.62	2.60 ± 0.30	2.46 ± 0.07[g]	≥4.54 ± 0.09	6.19 ± 0.16
U			2.9 ± 0.1[h]		

[a]Slope of linear least-squares trend line of $D_0(M^+-L)$ versus $D_0(L-L)$, Figure 6, forced to pass through the origin. [b]Ref 6. [c]Ref 15. [d]Ref 53. [e]Ref 25. [f]Ref 69. [g]Ref 87. [h]Ref 34.

DOI: 10.1021/acs.inorgchem.5b00137
Inorg. Chem. 2015, 54, 3584−3599

Table 6. Comparison of CCSD(T) Theoretical Results Using Several Basis Sets for Th^+ to Experimentally Measured Values (kJ/mol) along the Potential Energy Surface for Reaction 3[a]

	experimental	SDD[b]	ANO[c]	Seg. SDD[d]	KAP[e]
Th^+ ($^4F_{3/2}$) + CH_4[f]	0.0	0.0	0.0	0.0	0.0
Th^+ (^4F) + CH_4[g]	(5.8)	(28.9)	(16.4)	(18.3)	(11.6)
Th^+ ($^2D_{3/2}$) + CH_4[f]	22.2	−0.9	11.6	9.7	16.4
Th^+ (^2D) + CH_4[g]	(0.0)	(0.0)	(0.0)	(0.0)	(0.0)
^{4}1 (^{4}A″)	−45.3 ± 4.8	−46.9	−57.6	−47.5	−49.4
^{2}1 (^{2}A)		(−26.0)	(−53.6)	(−35.2)	(−39.6)
^{2}TS1/2 (^{2}A)[h]	16.4 ± 1.9	65.7	26.4	44.8	17.4
		(27.1)	(−12.2)	(6.2)	(−15.4)
$ThCH_2^+$ (^{2}A′) + H_2		15.9	−30.2	−13.0	−24.9
		(−22.7)	(−68.8)	(−51.6)	(−63.5)
MAD		19	8	11	3
		(22)	(12)	(11)	(11)

[a]Structures were optimized using B3LYP/SDD/6-311++G(d,p). Energies include estimated spin−orbit corrections and are relative to Th^+ ($^4F_{3/2}$, $6d^27s$) + CH_4. See the text. Values in parentheses are relative to Th^+ (^2D, $6d7s^2$) + CH_4 and do not include estimated spin−orbit corrections. [b]Single-point energy using SDD/6-311++G(3df,3p). [c]Single-point energy using (14s13p10d8f6g)/[6s6p5d4f3g] /6-311++G(3df,3p). [d]Single-point energies using (14s13p10d8f6g)/[10s9p5d4f3g]/6-311++G(3df,3p). [e]Structures were optimized at PBE0/(20s17p12d11f5g3h1i)/[7s7p6d5f5g3h1i]/cc-pVTZ. Single-point energies were performed with CCSD(T) utilizing the same basis sets. [f]Theoretical prediction of the lowest level in each state. Corrected from theoretical energy of each state by the empirical average excitation energy of that state, −44.4 kJ/mol for ^{4}F and −16.4 kJ/mol for ^{2}D. [g]Values in parentheses are averaged over all spin−orbit levels.[54,55] [h]Corrected by the empirical difference between ^{2}D averaged over all spin−orbit states and the $^4F_{3/2}$ level, 38.6 kJ/mol.

consistently higher than the other metal cation BDEs considered here with the possible exception of $D_0(Th^+-CH_2)$, which is only a lower limit. For the other BDEs, the Th^+ BDEs average 0.24 ± 0.16 eV higher in energy than the Zr^+ BDEs. Assuming that the trend between Th^+ and Zr^+ BDEs holds true for MCH_2^+, then $D_0(Th^+-CH_2)$ = 4.86 ± 0.17 eV can be estimated. This value is in reasonable agreement with BDEs obtained using the Seg. SDD basis set at the B3LYP (4.92 eV), B3PW91 (5.04 eV), and CCSD(T) (4.74 eV) levels as well as CCSD(T)/KAP (4.94 eV).

Spin−Orbit Corrected Potential Energy Surface. The kinetic energy dependent cross-section of reaction 3, Figure 1, clearly has an energy dependence inconsistent with a barrierless, simple exothermic reaction, as previously concluded on the basis of the FT-ICR experiments.[35,36] Thus, this reaction is either endothermic or a barrier in excess of the reactant energies is present. As noted above, before spin−orbit corrections, all levels of theory here, Table 4, and previous theoretical work[41,42] indicate that reaction 3 is exothermic overall; however, a valid comparison between experiment and theory requires consideration of a correction to account for spin−orbit interactions. (Ideally, this could be accomplished using either a two-component approach or a perturbative approach where matrix elements of the SOC Hamiltonian are computed between states that are low in energy. Here, we use a simpler first-order approximation to all spin−orbit corrections.) With the exception of intermediate **1**, all intermediates and transition states along the potential energy surface in Figure 4 are A states (including the $ThCH_2^+$ products discussed above) and as such should experience no first-order spin−orbit splitting. Furthermore, the quartet surface for this part of the potential energy surface is well above the doublet surface, such that spin−orbit interactions between these surfaces should also be relatively small. For intermediate **1**, an electrostatic interaction of Th^+ and CH_4, we expect a similar spin−orbit splitting as the unbound Th^+, which does exhibit spin−orbit interaction. As discussed above, this approximation leads to a calculated well depth for **1** relative to its respective asymptote remaining constant. To approximately correct the PES in Figure 4, we identify the true $J = {}^3/_2$ reactant asymptote as lying 38.4 kJ/mol (3211.991 cm^{-1}) lower in energy than the ^{2}D ($6d7s^2$) theoretical value, which is an average over all spin−orbit states of Th^+ (^{2}D). Likewise, the $^2D_{3/2}$ asymptote lies 16.2 kJ/mol (1352.053 cm^{-1}) below the ^{2}D. Referencing the PES to the $^4F_{3/2}$ asymptote pushes the energy of all intermediates (except **1**), transition states, and products up by 38.4 kJ/mol relative to Th^+ ($^4F_{3/2}$) + CH_4, as indicated by the solid line in Figure 4. Note that by using experimental spin−orbit splittings, we effectively include the mixing of the ^{4}F state into the reactants and intermediate **1** complex. Table 4 lists the explicit values of all species along the spin−orbit corrected PES at the CCSD(T) level shown in Figure 4, with results for other levels of theory in Table S7. Making this correction, B3LYP, B3PW91, and CCSD(T) levels predict that reaction 3 is exothermic by 13−39 kJ/mol, Table 4. (BHLYP predicts the reaction is endothermic by 16 kJ/mol, although, as noted above, BHLYP is not expected to be accurate for the multiply bound $ThCH_2^+$ product.)

A second corollary of the spin−orbit corrections is that a crossing between the quartet and doublet surfaces is observed between **1** and **^{2}TS1/2** at all levels of theory. de Almeida and Duarte also reported a crossing along their B3PW91 surface, Table 4, although it occurs between the Th^+ + CH_4 reactants and **1** and is a consequence of finding a Th^+ (^{4}F) ground state.[42] For the spin−orbit corrected surface shown in Figure 4, it can be realized that the surface crossing is an artifact of imposing the construct of a spin state on the reaction surface, whereas only the total spin−orbit quantum state is likely to be a good quantum number for such a heavy element. As a consequence, calculations designed to locate the crossing point would not be useful as there is no crossing between doublet and quartet surfaces before including spin−orbit corrections. In addition, experimentally, the $J = {}^3/_2$ ground level is a mixture of the ^{4}F and ^{2}D states so that **^{2}1** and **^{4}1** are both conceivably accessible directly from the ground level asymptote without a surface crossing.

DOI: 10.1021/acs.inorgchem.5b00137
Inorg. Chem. 2015, 54, 3584−3599

The presence of a barrier in excess of reactant energies is established experimentally by the CID of $ThCH_4^+$, Figure 3, which yields $Th^+ + CH_4$ exclusively. This result shows that the $ThCH_4^+$ adduct is trapped as the association intermediate **1**, $Th^+(CH_4)$. In previous work of the related platinum system, reaction of $Pt^+ + CH_4$ leads to dehydrogenation in a barrierless exothermic reaction and CID of $PtCH_4^+$ with Xe yielded $Pt^+ + CH_4$ and $PtH^+ + CH_3$ products, consistent with a $HPtCH_3^+$ structure.[22] Furthermore, the threshold measured for the $Pt^+ + CH_4$ products in the CID reaction, $E_0 = 1.72 \pm 0.05$ eV, is consistent with this inserted structure and much greater than would be expected for $Pt^+(CH_4)$, where theory predicts a threshold of $E_0 = 0.9$ eV. In the Th^+ system, if the barrier at ^{2}**TS1/2** were not present, the formation of ^{2}**2**, $HThCH_3^+$, would be expected as this is the most stable species on the reaction surface. Then, like the Pt^+ system, the CID products $ThCH_2^+ + H_2$ or $ThH^+ + CH_3$ should be observed at higher energies if $HThCH_3^+$ were present. Both of these products were explicitly looked for but not observed. Additionally, the threshold for forming the $Th^+ + CH_4$ products from **2** would be expected to be ~1 eV higher in energy than observed, Table 4.

When the PES is corrected for spin−orbit effects (ignoring any potential second order effects), all levels of theory predict a barrier for reaction 3 of 4−65 kJ/mol. The B3LYP and B3PW91 results indicate that the barrier results from spin−orbit effects. This is further substantiated by CCSD(T)/KAP calculations where no barrier is observed absent spin−orbit effects, but when spin−orbit effects are included, a barrier in excellent agreement with the threshold from reaction 3 is observed, Table 6. Furthermore, the difference in the computed barrier height at ^{2}**TS1/2** in the CH_4 and CD_4 systems is 5.7 kJ/mol, similar to the observed difference in the thresholds measured for reaction 3, 10.6 ± 3.5 kJ/mol. Given that the only product observed from the CID reaction is the loss of methane and that there is reasonable agreement between the theoretical barrier height and the experimental threshold, the threshold for reaction 3 is assigned to the barrier located at ^{2}**TS1/2**.

The presence of this barrier can be understood using a simple donor−acceptor model that predicts σ-bond activation requires an orbital on the thorium cation that can accept the electrons from the bond on the ligand to be broken. Furthermore, π-electrons on the metal backdonate into the antibonding orbital of the bond to be broken.[100] On the calculated potential surface for Th^+ (^{2}D, 6d7s^2), the 7s acceptor orbital is doubly occupied, leading to the repulsive interaction at **TS1/2**. By contrast, the ^{4}F (6d^{2}7s) has less electron density along the bond axis so that the interaction is less repulsive. The argument can be extended to a mixed electronic character $J = {}^3/_2$ (^{4}F,^{2}D) ground level of the ion, where the ^{2}D character increases the electron density in the 7s acceptor orbital such that a repulsive interaction still occurs.

To further understand the repulsive nature of the Th^+ ($J = {}^3/_2$) ground level interacting with CH_4, it is instructive to compare the potential energy surfaces of methane reacting with Zr^+,[15] Hf^+,[25] and Th^+. At the B3LYP/HW/6-311++G(3df,3p) and B3LYP/HW$^+$/6-311++G(3df,3p) levels of theory, the barrier height at **TS1/2** is 0 and 8 kJ/mol relative to the reactants for Zr^+[15] and Hf^+.[25] When spin−orbit corrections of 9 kJ/mol for Zr^+ and 21 kJ/mol for Hf^+ are made,[55] these barriers are 9 and 29 kJ/mol, respectively. The high barrier of Hf^+ has been ascribed to the filled 6s orbital of its ^{2}D (5d6s^2) ground state.[25] Zr^+ has a ^{4}F (4d^{2}5s) ground state and does not experience the same repulsive forces because of the half-filled 5s orbital.[15] The barrier height at **TS1/2** calculated using B3LYP for Th^+ is 18 kJ/mol, when using the similarly sized SDD basis set after accounting for spin−orbit energy. The observation that the **TS1/2** barrier for Th^+ lies in between those for Zr^+ and Hf^+ is consistent with the mixed electronic character of the Th^+ (^{4}F,^{2}D) ground level.

Basis Set Comparison. Theoretical calculations were performed using several basis sets for Th^+. The smallest of these basis sets, SDD, is double-ζ in quality and does not include polarization functions. Additionally, ANO and Seg. SDD basis sets from Cao et al.[71] that are quadruple-ζ in quality and include polarization *g*-functions and the KAP basis set that includes *g*-, *h*-, and *i*-functions were utilized. The results for the DFT calculations for the SDD, ANO, and Seg. SDD were similar for both the BDEs and PES calculated here, Tables S5 and S7, suggesting that there is little advantage in using the large basis set. For CCSD(T) calculations, the MADs found in Table S5 suggest that the SDD basis set performs the worst for BDEs but that there is little difference between the three larger basis sets. There is some indication that the larger basis sets perform better than SDD for the multiply bound species and worse than SDD for singly and electrostatically bound species for both DFT and CCSD(T) calculations.

In contrast to the DFT results, significant differences with basis set were observed in CCSD(T) calculations for the PES. A comparison of the energies from the CCSD(T) calculations using SDD, ANO, Seg. SDD, and KAP basis sets to the thresholds measured in reactions 3 and 7 can be found in Table 6. BDEs and full PESs with estimated spin−orbit corrections from the SDD, ANO, and Seg. SDD basis sets can be found in Tables S5 and S7 in the Supporting Information. As seen in Table 6, CCSD(T)/SDD calculations identify the ^{2}D (6d7s^2) (after averaging over all spin−orbit states) as the ground state, in agreement with the experimentally determined ground state, but they overestimate the difference between the ^{2}D and ^{4}F (6d^{2}7s) states by 23 kJ/mol. When spin−orbit corrections are applied, this level of theory incorrectly predicts the ground level as $^2D_{3/2}$. The use of the larger basis sets improves the agreement between theory and experiment, where deviations between theoretical and experimental spacing between the ^{2}D and ^{4}F states are 11, 12, and 6 kJ/mol for the ANO, Seg. SDD, and KAP basis sets, respectively. Furthermore, when spin−orbit effects are included, all three extended basis sets predict a $^4F_{3/2}$ ground level.

For the first intermediate, **1**, the CCSD(T) result when using the SDD basis set is within experimental uncertainty after including spin−orbit corrections. When the larger basis sets are used, ANO overestimates the well depth by 13 kJ/mol and the Seg. SDD and KAP are also within experimental uncertainty. However, although the SDD basis set performs reasonably well for **1**, it overestimates the barrier height at **TS1/2** by 49 kJ/mol. When using the larger basis sets, agreement with the threshold from reaction 3 improves to deviations of 10, 28, and 1 for ANO, Seg. SDD, and KAP, respectively. SDD also indicates that the reaction 3 is endothermic by 16 kJ/mol, whereas ANO, Seg. SDD, and KAP indicate that the reaction is exothermic by 30, 13, and 25 kJ/mol, respectively. Table 6 lists MADs for the CCSD(T) results using each basis set. These demonstrate that correcting for spin−orbit interactions generally improves agreement with the experimental results. This is most notable for the results obtained using the SDD and KAP basis sets. There is also significant improvement in agreement with the

DOI: 10.1021/acs.inorgchem.5b00137
Inorg. Chem. 2015, 54, 3584−3599

experimental results as the basis set gets larger, with MADs improving from 18 kJ/mol (SDD) to 8 and 11 kJ/mol for ANO and Seg. SDD, respectively, and the KAP basis set is in excellent agreement with all experimental values. As previously noted for Hf^+, the lack of polarization functions in CCSD(T) calculations leads to improper electron correlation calculations.[69] Thus, the inclusion of the polariztion *g*-functions in the Seg. SDD and ANO basis sets and of additional polarizing *g*-, *h*-, and *i*-functions in the KAP basis set significantly improves accuracy compared to experiment.

High-Energy Mechanisms. The cross-section for $ThCH_2^+$ in Figure 1 peaks at 2 eV and begins to fall off as the cross-sections for $ThCH_3^+$ and ThH^+ rise. Above 4 eV, ThH^+ dominates all other products. This is consistent with a common intermediate among the three species, which the calculations indicate is ^{2}**2**, $HThCH_3^+$. At high energies, it is kinetically more favorable to simply cleave a bond (loose transition state) as opposed to following the pathway through ^{2}**TS2/3** (tight transition state). Although $ThCH_3^+$ formation is slightly more favorable thermodynamically, the ThH^+ product dominates because angular momentum constraints necessitate that small impact parameters are required for $ThCH_3^+$ + H formation, whereas much larger impact parameters permit ThH^+ + CH_3 formation.[25] This constraint has been observed previously and explained thoroughly elsewhere.[14,88,101]

As noted above, reaction 6 occurs as the subsequent dehydrogenation of $ThCH_3^+$ produced from reaction 5. Other possible mechanisms are reactions 9 and 10.

$$Th^+ + CH_4 \rightarrow ThCH^+ + 3H \quad (9)$$

$$\rightarrow ThCH_2^+ + H_2 \rightarrow ThCH^+ + H + H_2 \quad (10)$$

Of these possible mechanisms, reaction 9 cannot occur until much higher energies, and reaction 10 is unlikely because reaction 4 is kinetically more favorable (see Figure 1) at energies near the reaction 6 threshold. The mechanism for the dehydrogenation of $ThCH_3^+$, reaction 6, is expected to be similar to the mechanism for reaction 3 observed in Figure 4, where H atoms from the CH_3 ligand are sequentially transferred to the metal to form an electrostatically bound $(H_2)ThCH^+$ complex that subsequently dissociates to products. According to this model, the first intermediate would be $HThCH_2^+$ (^{1}A′), which is only 1.0 kJ/mol higher in energy than the $ThCH_3^+$ (^{3}E) ground state (Table S4) according to B3LYP/SDD/6-311++G(d,p). This also necessitates a crossing seam between the triplet and singlet reaction surfaces in order to form ground-state $ThCH^+$ ($^1\Sigma^+$), although it seems unlikely that this would be restrictive given the extensive spin−orbit coupling in Th^+. Also according to CCSD(T) theory, the ground state of $ThCH_3^+$ is actually $^1A_1$, which could dehydrogenate in a spin-allowed process. Note that both states of $ThCH_3^+$ can be formed in spin-allowed processes from the $HThCH_3^+$ (^{2}A′) intermediate, Figure 4.

CONCLUSIONS

The reaction of methane with thorium cation produces several products over a wide energy range. The dominant product at low energies is the thorium carbene cation; however, the energy dependence of this product is inconsistent with that of a barrierless exothermic reaction. Theory coupled with careful examination of spin−orbit interactions suggests that the threshold of this reaction corresponds to a barrier found in the first transition state associated with C−H bond activation. This is further substantiated by the CID reaction of the thorium−methane adduct, which dissociates exclusively to form the atomic Th^+ ion and methane. The barrier likely exists because the ground $J = {}^3/_2$ level has mixed electronic character in which the closed $7s^2$ shell character of the ^{2}D ($6d7s^2$) hinders bond activation. Importantly, the barrier disappears at most levels of theory when spin−orbit interactions are not included such that spin−orbit effects are critical to understanding the observed experimental behavior.

At higher energies, the thorium hydride cation product dominates, although the thorium methyl product has a similar threshold. These products are kinetically favored once the endothermicity is overcome because they require a simple bond cleavage of the hydrido-methyl thorium cation as opposed to the molecular rearrangement needed for dehydrogenation. Meanwhile, the ThH^+ channel is favored over the $ThCH_3^+$ channel because of angular momentum constraints.[14,88,101]

Thorium's electronic structure is unique among the actinides because the f-orbitals are unoccupied for the neutral and singly charged cation. By all accounts, Th^+ is more comparable to Ti^+, Zr^+, and Hf^+, which also have three valence electrons. Th^+ BDEs are typically stronger than the BDEs of its congeners, consistent with the assumption that BDEs increase moving down the periodic table because of a lanthanide contraction effect.[22,23,26,27,89] This indicates that although the mixed character ground level of the Th^+ plays a significant role in the Th^+ + CH_4 reaction surface (i.e., the barrier at **TS1/2**) it hampers Th^+ bonding only slightly.

ASSOCIATED CONTENT

Supporting Information

Ion electronic population analysis, neutral BDEs of CH_4 and CD_4, reaction cross-section as a function of kinetic energy of Th^+ + CH_4, evaluation of ζ_{6d}(Th), comparison of Th^+ theoretical energies with several additional basis sets, theoretical energies of all calculated structures, and $ThCH_x^+$ BDEs with several additional basis sets. This material is available free of charge via the Internet at http://pubs.acs.org.

AUTHOR INFORMATION

Corresponding Author

*E-mail: armentrout@chem.utah.edu.

Notes

The authors declare no competing financial interest.

ACKNOWLEDGMENTS

This work was supported by the Heavy Element Chemistry Program, Office of Basic Energy Sciences, U.S. Department of Energy, grant no. DE-SC0012249. We thank the Center for High Performance Computing at the University of Utah for the generous allocation of computer time. This research used resources of the Oak Ridge Leadership Computing Facility, which is a DOE Office of Science User Facility supported under contract DE-AC05-00OR22725. An award of computer time was provided by the Innovative and Novel Computational Impact on Theory and Experiment (INCITE) program. Professor Michael Morse is thanked for several useful conversations regarding the estimation of spin−orbit corrections.

DOI: 10.1021/acs.inorgchem.5b00137
Inorg. Chem. 2015, 54, 3584−3599

REFERENCES

(1) Shayesteh, A.; Lavrov, V. V.; Koyanagi, G. K.; Bohme, D. K. *J. Phys. Chem. A* **2009**, *113*, 5602−5611.
(2) Roithová, J.; Schröder, D. *Chem. Rev.* **2010**, *110*, 1170−1211.
(3) Schwarz, H. *Angew. Chem., Int. Ed.* **2011**, *50*, 10096−10115.
(4) Haggin, J. *Chem. Eng. News* **1993**, *71*, 22−23.
(5) Halle, L. F.; Armentrout, P. B.; Beauchamp, J. L. *J. Am. Chem. Soc.* **1981**, *103*, 962−963.
(6) Sunderlin, L. S.; Armentrout, P. B. *J. Phys. Chem.* **1988**, *92*, 1209−1219.
(7) Sunderlin, L. S.; Armentrout, P. B. *J. Am. Chem. Soc.* **1989**, *111*, 3845−3855.
(8) Schröder, D.; Schwarz, H.; Clemmer, D. E.; Chen, Y.; Armentrout, P. B.; Baranov, V. I.; Bohme, D. K. *Int. J. Mass Spectrom. Ion Processes* **1997**, *161*, 175−191.
(9) Aristov, N.; Armentrout, P. B. *J. Phys. Chem.* **1987**, *91*, 6178−6188.
(10) Georgiadis, R.; Armentrout, P. B. *J. Phys. Chem.* **1988**, *92*, 7067−7074.
(11) Haynes, C. L.; Chen, Y.-M.; Armentrout, P. B. *J. Phys. Chem.* **1995**, *99*, 9110−9117.
(12) Liu, F.; Zhang, X.-G.; Armentrout, P. B. *Phys. Chem. Chem. Phys.* **2005**, *7*, 1054−1064.
(13) Mandich, M. L.; Halle, L. F.; Beauchamp, J. L. *J. Am. Chem. Soc.* **1984**, *106*, 4403−4411.
(14) Chen, Y.-M.; Armentrout, P. B. *J. Phys. Chem.* **1995**, *99*, 10775−10779.
(15) Armentrout, P. B.; Sievers, M. R. *J. Phys. Chem. A* **2003**, *107*, 4396−4406.
(16) Armentrout, P. B. *J. Phys. Chem. A* **2006**, *110*, 8327−8338.
(17) Schultz, R. H.; Elkind, J. L.; Armentrout, P. B. *J. Am. Chem. Soc.* **1988**, *110*, 411−423.
(18) Chen, Y.-M.; Sievers, M. R.; Armentrout, P. B. *Int. J. Mass Spectrom. Ion Processes* **1997**, *167/168*, 195−212.
(19) Sievers, M. R.; Chen, Y.-M.; Haynes, C. L.; Armentrout, P. B. *Int. J. Mass Spectrom.* **2000**, *195/196*, 149−170.
(20) Irikura, K. K.; Beauchamp, J. L. *J. Phys. Chem.* **1991**, *95*, 8344−8351.
(21) Irikura, K. K.; Beauchamp, J. L. *J. Am. Chem. Soc.* **1991**, *113*, 2769−2770.
(22) Zhang, X.-G.; Liyanage, R.; Armentrout, P. B. *J. Am. Chem. Soc.* **2001**, *123*, 5563−5575.
(23) Armentrout, M. M.; Li, F.-X.; Armentrout, P. B. *J. Phys. Chem. A* **2004**, *108*, 9660−9672.
(24) Li, F.-X.; Armentrout, P. B. *J. Chem. Phys.* **2006**, *125*, 133114.
(25) Parke, L. G.; Hinton, C. S.; Armentrout, P. B. *Int. J. Mass Spectrom.* **2006**, *254*, 168−182.
(26) Armentrout, P. B.; Shin, S.; Liyanage, R. *J. Phys. Chem. A* **2006**, *110*, 1242−1260.
(27) Li, F.-X.; Zhang, X.-G.; Armentrout, P. B. *Int. J. Mass Spectrom.* **2006**, *255*−*256*, 279−300.
(28) Parke, L. G.; Hinton, C. S.; Armentrout, P. B. *J. Phys. Chem. C* **2007**, *111*, 17773−17787.
(29) Parke, L. G.; Hinton, C. S.; Armentrout, P. B. *J. Phys. Chem. A* **2008**, *112*, 10469−10480.
(30) Armentrout, P. B.; Parke, L.; Hinton, C.; Citir, M. *ChemPlusChem* **2013**, *78*, 1157−1173.
(31) Schilling, J. B.; Beauchamp, J. L. *J. Am. Chem. Soc.* **1988**, *110*, 15−24.
(32) Cornehl, H. H.; Heinemann, C.; Schroeder, D.; Schwarz, H. *Organometallics* **1995**, *14*, 992−999.
(33) Marcalo, J.; Santos, M.; Pires de Matos, A.; Gibson, J. K.; Haire, R. G. *J. Phys. Chem. A* **2008**, *112*, 12647−12656.
(34) Armentrout, P. B.; Hodges, R. V.; Beauchamp, J. L. *J. Chem. Phys.* **1977**, *66*, 4683−4688.
(35) Marçalo, J.; Leal, J. P.; Pires de Matos, A. *Int. J. Mass Spectrom. Ion Processes* **1996**, *157/158*, 265−274.
(36) Gibson, J. K.; Haire, R. G.; Marçalo, J.; Santos, M.; Pires de Matos, A.; Mrozik, M. K.; Pitzer, R. M.; Bursten, B. E. *Organometallics* **2007**, *26*, 3947−3956.
(37) Cornehl, H. H.; Wesendrup, R.; Diefenbach, M.; Schwarz, H. *Chem.—Eur. J.* **1997**, *3*, 1083−1090.
(38) Gibson, J. K.; Haire, R. G. *Inorg. Chem.* **2002**, *41*, 5897−5906.
(39) Marcalo, J.; Gibson, J. K. *J. Phys. Chem. A* **2009**, *113*, 12599−12606.
(40) Su, T.; Chesnavich, W. J. *J. Chem. Phys.* **1982**, *76*, 5183−5185.
(41) Di Santo, E.; Michelini, M. d. C.; Russo, N. *Organometallics* **2009**, *28*, 3716−3726.
(42) de Almeida, K. J.; Duarte, H. A. *Organometallics* **2010**, *29*, 3735−3745.
(43) Loh, S. K.; Hales, D. A.; Li, L.; Armentrout, P. B. *J. Chem. Phys.* **1989**, *90*, 5466−5485.
(44) Schultz, R. H.; Armentrout, P. B. *Int. J. Mass Spectrom. Ion Processes* **1991**, *107*, 29−48.
(45) Gerlich, D. *Adv. Chem. Phys.* **1992**, *82*, 1−176.
(46) Armentrout, P. B. *Int. J. Mass Spectrom.* **2000**, *200*, 219−241.
(47) Ervin, K. M.; Armentrout, P. B. *J. Chem. Phys.* **1985**, *83*, 166−189.
(48) Daly, N. R. *Rev. Sci. Instrum.* **1960**, *31*, 264−267.
(49) Haynes, C. L.; Armentrout, P. B. *Organometallics* **1994**, *13*, 3480−3490.
(50) Clemmer, D. E.; Chen, Y.-M.; Khan, F. A.; Armentrout, P. B. *J. Phys. Chem.* **1994**, *98*, 6522−6529.
(51) Kickel, B. L.; Armentrout, P. B. *J. Am. Chem. Soc.* **1995**, *117*, 764−773.
(52) Kickel, B. L.; Armentrout, P. B. *J. Am. Chem. Soc.* **1995**, *117*, 4057−4070.
(53) Sievers, M. R.; Chen, Y.-M.; Elkind, J. L.; Armentrout, P. B. *J. Phys. Chem.* **1996**, *100*, 54−62.
(54) Blaise, J.; Wyart, J.-F. *Selected Constants, Energy Levels, and Atomic Spectra of Actinides*; http://web2.lac.u-psud.fr/lac/Database/Contents.html.
(55) Sansonetti, J. E.; Martin, W. C. *J. Phys. Chem. Ref. Data* **2005**, *34*, 1559−2259.
(56) Chesnavich, W. J.; Bowers, M. T. *J. Phys. Chem.* **1979**, *83*, 900−905.
(57) Muntean, F.; Armentrout, P. B. *J. Chem. Phys.* **2001**, *115*, 1213−1228.
(58) Aristov, N.; Armentrout, P. B. *J. Am. Chem. Soc.* **1986**, *108*, 1806−1819.
(59) Armentrout, P. B. In *Advances in Gas Phase Ion Chemistry*; Adams, N., Babcock, L. M., Eds.; JAI Press: Greenwich, CT, 1992; Vol. *1*, pp 83−119.
(60) *NIST Computational Chemistry Comparison and Benchmark Database; NIST Standard Reference Database Number 101 Release 16a*; Johnson, R. D., III, Ed.; August 2013; http://cccbdb.nist.gov/
(61) Frisch, M. J.; Trucks, G. W.; Schlegel, H. B.; Scuseria, G. E.; Robb, M. A.; Cheeseman, J. R.; Scalmani, G.; Barone, V.; Mennucci, B.; Petersson, G. A.; Nakatsuji, H.; Caricato, M.; Li, X.; Hratchian, H. P.; Izmaylov, A. F.; Bloino, J.; Zheng, G.; Sonnenberg, J. L.; Hada, M.; Ehara, M.; Toyota, K.; Fukuda, R.; Hasegawa, J.; Ishida, M.; Nakajima, T.; Honda, Y.; Kitao, O.; Nakai, H.; Vreven, T.; Montgomery, J. A., Jr.; Peralta, J. E.; Ogliaro, F.; Bearpark, M.; Heyd, J. J.; Brothers, E.; Kudin, K. N.; Staroverov, V. N.; Kobayashi, R.; Normand, J.; Raghavachari, K.; Rendell, A.; Burant, J. C.; Iyengar, S. S.; Tomasi, J.; Cossi, M.; Rega, N.; Millam, N. J.; Klene, M.; Knox, J. E.; Cross, J. B.; Bakken, V.; Adamo, C.; Jaramillo, J.; Gomperts, R.; Stratmann, R. E.; Yazyev, O.; Austin, A. J.; Cammi, R.; Pomelli, C.; Ochterski, J. W.; Martin, R. L.; Morokuma, K.; Zakrzewski, V. G.; Voth, G. A.; Salvador, P.; Dannenberg, J. J.; Dapprich, S.; Daniels, A. D.; Farkas, Ö.; Foresman, J. B.; Ortiz, J. V.; Cioslowski, J.; Fox, D. J. *Gaussian 09*; Gaussian, Inc: Wallingford, CT, 2009.
(62) Lee, C.; Yang, W.; Parr, R. G. *Phys. Rev. B: Condens. Matter* **1988**, *37*, 785−789.
(63) Becke, A. D. *J. Chem. Phys.* **1993**, *98*, 5648−5652.

DOI: 10.1021/acs.inorgchem.5b00137
Inorg. Chem. 2015, 54, 3584−3599

(64) Kuechle, W.; Dolg, M.; Stoll, H.; Preuss, H. *J. Chem. Phys.* **1994**, *100*, 7535−7542.
(65) Pople, J. A.; Head-Gordon, M.; Raghavachari, K. *J. Chem. Phys.* **1987**, *87*, 5968−5975.
(66) Feller, D. *J. Comput. Chem.* **1996**, *17*, 1571−1586.
(67) Schuchardt, K. L.; Didier, B. T.; Elsethagen, T.; Sun, L.; Gurumoorthi, V.; Chase, J.; Li, J.; Windus, T. L. *J. Chem. Inf. Model.* **2007**, *47*, 1045−1052.
(68) Hinton, C. S.; Li, F.; Armentrout, P. B. *Int. J. Mass Spectrom.* **2009**, *280*, 226−234.
(69) Hinton, C. S.; Armentrout, P. B. *J. Chem. Phys.* **2010**, *133*, 124307.
(70) Hinton, C. S.; Citir, M.; Armentrout, P. B. *J. Chem. Phys.* **2011**, *135*, 234302.
(71) Cao, X.; Dolg, M.; Stoll, H. *J. Chem. Phys.* **2003**, *118*, 487−496.
(72) Holthausen, M. C.; Heinemann, C.; Cornehl, H. H.; Koch, W.; Schwarz, H. *J. Chem. Phys.* **1995**, *102*, 4931−4941.
(73) Cizek, J. In *Advances in Chemical Physics*; Hariharan, P. C., Ed.; Wiley Interscience: New York, 1969; Vol. *14*, p 35.
(74) Purvis, G. D., III; Bartlett, R. J. *J. Chem. Phys.* **1982**, *76*, 1910−1918.
(75) Scuseria, G. E.; Janssen, C. L.; Schaefer, H. F., III *J. Chem. Phys.* **1988**, *89*, 7382−7387.
(76) Foresman, J. B.; Frisch, A. E. *Exploring Chemistry with Electronic Structure Methods*, 2nd ed.; Gaussian, Inc.: Pittsburgh, PA, 1996.
(77) Peng, C.; Schlegel, H. B. *Isr. J. Chem.* **1994**, *33*, 449−454.
(78) Peng, C.; Ayala, P.; Schlegel, H. B.; Frisch, M. J. *J. Comput. Chem.* **1996**, *17*, 49−56.
(79) Valiev, M.; Bylaska, E. J.; Govind, N.; Kowalski, K.; Straatsma, T. P.; Van Dam, H. J. J.; Wang, D.; Nieplocha, J.; Apra, E.; Windus, T. L.; de Jong, W. A. *Comput. Phys. Commun.* **2010**, *181*, 1477−1489.
(80) Weigand, A.; Cao, X.; Hangele, T.; Dolg, M. *J. Phys. Chem. A* **2014**, *118*, 2519−2530.
(81) Peterson, K. A. to be submitted for publication.
(82) Dunning, T. H. *J. Chem. Phys.* **1989**, *90*, 1007.
(83) Adamo, C.; Barone, V. *J. Chem. Phys.* **1999**, *110*, 6158−6170.
(84) Jonsson, H.; Mills, G.; Jacobsen, K. W. In *Classical and Quantum Dynamics in Condensed Phase Simulations*; Berne, B. J., Ciccotti, G., Coker, D. F., Eds.; World Scientific: River Edge, NJ, 1998; p 385.
(85) Lapoutre, V. J. F.; Redlich, B.; van der Meer, A. F. G.; Oomens, J.; Bakker, J. M.; Sweeney, A.; Mookherjee, A.; Armentrout, P. B. *J. Phys. Chem. A* **2013**, *117*, 4115−4126.
(86) Armentrout, P. B.; Li, F.-X. *J. Chem. Phys.* **2004**, *121*, 248−256.
(87) Cox, R.; Armentrout, P. B. unpublished work.
(88) Sunderlin, L. S.; Armentrout, P. B. *J. Phys. Chem.* **1988**, *92*, 1209−1219.
(89) Zhang, X.; Schwarz, H. *Chem.—Eur. J.* **2010**, *16*, 5882−5888.
(90) Rodgers, M. T.; Armentrout, P. B. *J. Chem. Phys.* **1998**, *109*, 1787−1800.
(91) Armentrout, P. B.; Ervin, K. M.; Rodgers, M. T. *J. Phys. Chem. A* **2008**, *112*, 10071−10085.
(92) Rodgers, M. T.; Ervin, K. M.; Armentrout, P. B. *J. Chem. Phys.* **1997**, *106*, 4499−4508.
(93) Gilbert, R. G.; Smith, S. C. *Theory of Unimolecular and Recombination Reactions*; Blackwell Scientific: Oxford, 1990.
(94) Holbrook, K. A.; Pilling, M. J.; Robertson, S. H. *Unimolecular Reactions*; Wiley: New York, 1996.
(95) Heaven, M. C.; Barker, B. J.; Antonov, I. O. *J. Phys. Chem. A* **2014**, *118*, 10867−10881.
(96) Garcia, M. A.; Morse, M. D. *J. Chem. Phys.* **2011**, *135*, 114304.
(97) Armentrout, P. B. *J. Chem. Phys.* **2013**, *139*, 084305.
(98) Armentrout, P. B.; Li, F.-X. *J. Phys. Chem. A* **2013**, *117*, 7754−7766.
(99) Lefebvre-Brion, H.; Field, R. W. *The Spectra And Dynamics of Diatomic Molecules*; Elsevier: Amsterdam, 2004.
(100) Armentrout, P. B. In *Topics in Organometallic Chemistry*; Brown, J. M., Hofmann, P., Eds.; Springer-Verlag: Berlin, 1999; Vol. *4*, pp 1−45.
(101) Armentrout, P. B.; Kickel, B. L. In *Organometallic Ion Chemistry*; Freiser, B. S., Ed.; Kluwer: Dordrecht, The Netherlands, 1996; pp 1−45.

DOI: 10.1021/acs.inorgchem.5b00137
Inorg. Chem. 2015, 54, 3584−3599